Earth Surf. Dynam., 2, 383–401, 2014
www.earth-surf-dynam.net/2/383/2014/
doi:10.5194/esurf-2-383-2014

Earth Surface Dynamics
Open Access

Arctic–alpine blockfields in the northern Swedish Scandes: late Quaternary – not Neogene

B. W. Goodfellow[1,2], A. P. Stroeven[1], D. Fabel[3], O. Fredin[4,5], M.-H. Derron[5,6], R. Bintanja[7], and M. W. Caffee[8]

[1]Department of Physical Geography and Quaternary Geology, and Bolin Centre for Climate Research, Stockholm University, 10691 Stockholm, Sweden
[2]Department of Geology, Lund University, 22362 Lund, Sweden
[3]Department of Geographical and Earth Sciences, East Quadrangle, University Avenue, University of Glasgow, Glasgow G12 8QQ, UK
[4]Department of Geography, Norwegian University of Science and Technology (NTNU),7491, Trondheim, Norway
[5]Geological Survey of Norway, Leiv Eirikssons vei 39, 7491 Trondheim, Norway
[6]Institute of Geomatics and Risk Analysis, University of Lausanne, 1015 Lausanne, Switzerland
[7]Royal Netherlands Meteorological Institute, Wilhelminalaan 10, 3732 GK De Bilt, the Netherlands
[8]Department of Physics, Purdue University, West Lafayette, Indiana, USA

Correspondence to: B. W. Goodfellow (brad.goodfellow@natgeo.su.se)

Received: 22 January 2014 – Published in Earth Surf. Dynam. Discuss.: 10 February 2014
Revised: 9 June 2014 – Accepted: 24 June 2014 – Published: 21 July 2014

Abstract. Autochthonous blockfield mantles may indicate alpine surfaces that have not been glacially eroded. These surfaces may therefore serve as markers against which to determine Quaternary erosion volumes in adjacent glacially eroded sectors. To explore these potential utilities, chemical weathering features, erosion rates, and regolith residence durations of mountain blockfields are investigated in the northern Swedish Scandes. This is done, firstly, by assessing the intensity of regolith chemical weathering along altitudinal transects descending from three blockfield-mantled summits. Clay / silt ratios, secondary mineral assemblages, and imaging of chemical etching of primary mineral grains in fine matrix are each used for this purpose. Secondly, erosion rates and regolith residence durations of two of the summits are inferred from concentrations of in situ-produced cosmogenic ^{10}Be and ^{26}Al in quartz at the blockfield surfaces. An interpretative model is adopted that includes temporal variations in nuclide production rates through surface burial by glacial ice and glacial isostasy-induced elevation changes of the blockfield surfaces. Together, our data indicate that these blockfields are not derived from remnants of intensely weathered Neogene weathering profiles, as is commonly considered. Evidence for this interpretation includes minor chemical weathering in each of the three examined blockfields, despite consistent variability according to slope position. In addition, average erosion rates of ~ 16.2 and $\sim 6.7\,\mathrm{mm\,ka^{-1}}$, calculated for the two blockfield-mantled summits, are low but of sufficient magnitude to remove present blockfield mantles, of up to a few metres in thickness, within a late Quaternary time frame. Hence, blockfield mantles appear to be replenished by regolith formation through, primarily physical, weathering processes that have operated during the Quaternary. The persistence of autochthonous blockfields over multiple glacial–interglacial cycles confirms their importance as key markers of surfaces that were not glacially eroded through, at least, the late Quaternary. However, presently blockfield-mantled surfaces may potentially be subjected to large spatial variations in erosion rates, and their Neogene regolith mantles may have been comprehensively eroded during the late Pliocene and early Pleistocene. Their role as markers by which to estimate glacial erosion volumes in surrounding landscape elements therefore remains uncertain.

1 Introduction

Autochthonous blockfields are diamicts comprised of clay- to boulder-sized regolith formed through in situ bedrock weathering (Potter and Moss, 1968; Nesje et al., 1988; Ballantyne, 1998; Boelhouwers, 2004). They are classically a feature of periglaciated landscapes, where they frequently mantle mountain summits and plateaus assumed to have undergone up to tens of metres of (non-glacial) erosion during the Quaternary (Dahl, 1966; Ives, 1966; Sugden, 1968, 1974; Nesje et al., 1988; Rea et al., 1996; Ballantyne, 1998; Small et al., 1999; Goodfellow et al., 2009; Rea, 2013). According to this interpretation, blockfields indicate surfaces that persisted as nunataks or were inundated by non-erosive cold-based ice during glacial periods. Blockfield-mantled surfaces may provide useful markers for quantifying Quaternary glacial erosion volumes in surrounding landscapes (Nesje and Whillans, 1994; Glasser and Hall, 1997; Kleman and Stroeven, 1997; Staiger et al., 2005; Goodfellow, 2007; Jansson et al., 2011). However, recent studies of landscape evolution and Quaternary sediment budgets along the Norwegian margin (Nielsen et al., 2009; Steer et al., 2012) imply that, rather than providing these markers, autochthonous blockfield-mantled surfaces have also undergone surface lowering of some hundreds of metres through the action of a Quaternary glacial and periglacial "buzz saw". The origins, ages, and erosion rates of blockfields remain enigmatic, so their utility for indicating non-glacially eroded surfaces and for estimating Quaternary erosion volumes is contentious. The weathering characteristics, erosion rates, and residence durations of present autochthonous blockfield regoliths in the periglaciated northern Scandinavian Mountains (Scandes) are investigated in this study.

Autochthonous blockfields in periglaciated landscapes are frequently hypothesized to be remnants of Neogene weathering profiles (Caine, 1968; Ives, 1974; Clapperton, 1975; Nesje et al., 1988; Rea et al., 1996; Boelhouwers et al., 2002; André, 2003; Marquette et al., 2004; Sumner and Meiklejohn, 2004; Fjellanger et al., 2006; Paasche et al., 2006; André et al., 2008; Strømsøe and Paasche, 2011). In this model, block production is initiated through chemical weathering of bedrock during the Neogene by a warmer-than-present climate. Regolith stripping occurred during the colder Quaternary, subaerially exposing rock made more porous by chemical weathering. Enhanced access by water permitted efficient frost shattering of this rock, which was periglacially reworked to produce blockfield mantles that armour these surfaces, making them resistant to further modification (Boelhouwers, 2004).

If chemical weathering depends upon a "warm" climate, certain characteristics of blockfields are incompatible with a Quaternary origin. These characteristics include the presence of saprolite (Caine, 1968) and/or secondary minerals, especially kaolinite and gibbsite (Rea et al., 1996; Fjellanger et al., 2006; André et al., 2008; Strømsøe and Paasche, 2011), and clay abundances exceeding about 10 % of the fine matrix (clay, silt, sand) by volume (Rea et al., 1996; Strømsøe and Paasche, 2011). An additional circumstantial argument is that there are apparently no actively forming blockfields (Boelhouwers, 2004), with the exception of those developing on highly frost susceptible limestone in the Canadian Arctic (Dredge, 1992). Also, blockfield-mantled surface remnants do not appear to have been glacially eroded (Sugden, 1968, 1974; Kleman and Stroeven, 1997; Fabel et al., 2002; Marquette et al., 2004; Stroeven et al., 2006; Goodfellow, 2007). Taken together, the evidence seemingly indicates that blockfields may pre-date the last glacial–interglacial cycle. Field observations in conjunction with geochemical features may indicate regolith residence durations extending back into the Neogene (Rea et al., 1996; Whalley et al., 2004; André et al., 2008; Strømsøe and Paasche, 2011).

The Neogene-origin model is not universally accepted, and some researchers conclude that blockfields in periglaciated landscapes are entirely Quaternary features (Dahl, 1966; Dredge, 1992; Ballantyne, 1998, 2010; Ballantyne et al., 1998; Goodfellow et al., 2009; Goodfellow, 2012). In this model, blockfields are produced through synergistic physical (e.g. through frost-cracking) and chemical weathering processes (Whalley et al., 2004) that operate independently of preconditioning by Neogene processes.

Key evidence supporting the Quaternary-origin model includes slow formation of clay-sized regolith and secondary minerals through chemical weathering. This is indicated, firstly, by a low ratio of clay to silt across a sample batch (clay$< \sim 0.5 \times$ silt), compared with higher ratios (clay$> \sim 0.5 \times$ silt) in regoliths located in non-periglaciated settings (Goodfellow, 2012). Secondly, low abundances of secondary minerals are mixed in with abundant primary minerals (Goodfellow, 2012). The secondary mineral assemblages may span a range of leaching intensities including low (minerals with interstratified primary and secondary layers), moderate (2 : 1 layer minerals such as vermiculite), high (1 : 1 minerals such as kaolinite), and extreme (Al- and Fe-oxides such as gibbsite and haematite). This may reflect the effect of hydrological heterogeneities on weathering intensity in blockfields and the varying susceptibility of different primary minerals to chemical weathering. These mineral assemblages differ from those occurring in subtropical and tropical regoliths, which are generally simpler and dominated by high volumes (i.e. > 30 % of the regolith) of kaolinite and Al- and Fe-oxides (Meunier et al., 2007; White et al., 1998; Goodfellow, 2012).

In the Quaternary-origin model, it is further argued that blocks form by frost cracking *within* the regolith, near the base of the permafrost active layer where liquid water accumulates and seasonally refreezes (Dahl, 1966; Anderson,

1998; Small et al., 1999; Hales and Roering, 2007; Goodfellow et al., 2009; Ballantyne, 2010). This mechanism might therefore explain the apparent absence of frost cracking of clasts comprising blockfield surfaces while further highlighting a possible key role of Quaternary, rather than Neogene, weathering processes in blockfield formation.

A critical problem with ascertaining blockfield ages and origins is that it has, until recently, been impossible to measure blockfield erosion rates or regolith residence durations. However, measurements of terrestrial cosmogenic nuclide (TCN) concentrations now offer some insight into these issues. Erosion rates of 1.1–12.0 mm ka^{-1} have been inferred for subaerially exposed bedrock within alpine blockfields (Small et al., 1997; Bierman et al., 1999; Staiger et al., 2005; Phillips et al., 2006). These rates may be lower than in the surrounding blockfields, because exposed bedrock sheds, rather than retains, water (Small et al., 1999; Cockburn and Summerfield, 2004; Phillips et al., 2006). However, regolith erosion rates in summit blockfields may remain low because of armouring of gently sloping surfaces by cobbles and boulders (Granger et al., 2001; Boelhouwers, 2004). For example, erosion rates of 13.4–14.0 mm ka^{-1} have been measured in plateau blockfields in the Wind River Range, Wyoming, which have not been inundated by glacial ice (Small et al., 1999). Where non-erosive cold-based ice has buried blockfields during glacial periods (Sugden and Watts, 1977; Kleman and Stroeven, 1997; Bierman et al., 1999; Hättestrand and Stroeven, 2002; Briner et al., 2003; Marquette et al., 2004), time-averaged erosion rates are further lowered. Subaerial exposure and burial durations of blockfield regoliths might then extend back in time to the early Quaternary or late Neogene. By combining measurements of TCN concentrations in bedrock or regolith with an inferred history of surface burial by ice sheets from benthic δ^{18}O records (Fabel et al., 2002; Stroeven et al., 2002; Li et al., 2008), it is possible to estimate minimum time spans over which present blockfield regoliths have mantled surfaces (i.e. minimum regolith residence durations).

In this study we test whether blockfields in the northern Swedish Scandes are remnants of intensely weathered Neogene regoliths or are formed solely by Quaternary weathering processes. We do this, firstly, by investigating the intensity of chemical weathering through grain size, X-ray diffraction, and scanning electron microscopy (SEM) analyses of blockfield fine matrix along three hillslope transects. Secondly, we examine regolith residence durations of two summit blockfields through the combination of apparent surface exposure durations, measured through TCN analyses, with burial durations, determined through an ice sheet model driven by benthic δ^{18}O records. Incorporating an elastic lithosphere, relaxed asthenosphere (ELRA) bedrock model, the ice sheet model is also used to study the effects of bedrock isostatic response to glacial loading and unloading on nuclide production rates (which vary with elevation above sea level) and subsequent regolith residence durations. Because uncertainties associated with calculations of regolith residence durations are large, we confine our enquiry to an order of magnitude question: are regolith residence durations likely confined to the late Quaternary (< 1 Ma) or do they extend to the early Quaternary/late Neogene? A Neogene origin would imply low Quaternary-averaged surface erosion rates and a utility of autochthonous blockfield-mantled surfaces as markers from which to estimate glacial erosion depths in surrounding landscapes. In contrast, the implications of a Quaternary origin are more ambiguous. These could not exclude tens of metres, to perhaps more than one hundred metres, of surface lowering during the Plio-Pleistocene transition of currently blockfield-mantled surfaces, resulting in a lowered utility of these surfaces as markers from which to estimate glacial erosion depths in surrounding landscape sectors.

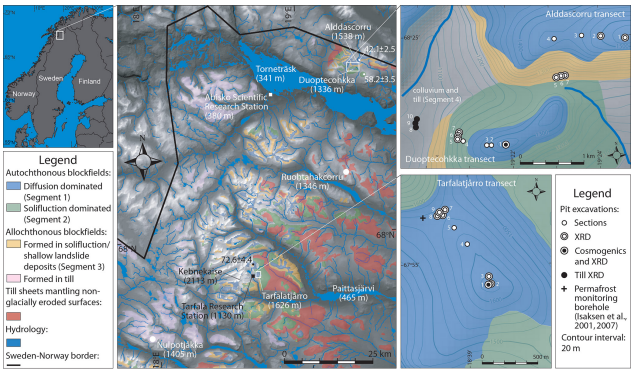

Figure 1. Map of the study areas in the northern Swedish Scandes. The map location and sample sites along three hillslope transects are shown in the adjoining panels. Autochthonous blockfields mantling low-gradient convex summits appear to be eroded by diffusive processes, such as regolith creep, and erosion of autochthonous blockfields on steep slopes appears dominated by solifluction. Colluvial boulder drapes provide evidence of shallow landsliding and form allochthonous blockfields on the steepest regolith-mantled slopes. These comprise slope segments 1, 2, and 3, respectively, and are the focus of regolith sampling in this study. Allochthonous blockfields also form in till sheets ($< \sim 1$ m thick) deposited on some glacially eroded summits (Goodfellow et al., 2008) and on some high-altitude non-glacially eroded surface remnants (Kleman and Stroeven, 1997; Fabel et al., 2002; Goodfellow et al., 2008). Pits along each transect are numbered according to those given in Tables 1 and 2 and S1 in the Supplement. Grey areas of the maps are cliff faces, talus slopes, or surfaces modified by glacial erosion or deposition (covered in $> \sim 1$ m thick tills on the transect maps). In the top right panel, mixed colluvium and till drape the landscape below Alddasčorru and Duoptečohkka in the grey area west of these summits and comprises segment 4 for regolith sampling in this study. ^{10}Be bedrock exposure ages from sites close to those used in this study are reproduced from Fabel et al. (2002) and Stroeven et al. (2006).

2 Study area

Blockfields were examined along hillslope transects descending from three summits in the northern Swedish Scandes (Fig. 1): Alddasčorru (68°25′ N, 19°24′ E; 1538 m above sea level (a.s.l.)), Duoptečohkka (68°24′ N, 19°22′ E; 1336 m a.s.l.), and Tarfalatjårro (67°55′ N, 18°39′ E; 1626 m a.s.l.). The transects intersect slope segments shaped by contrasting assemblages of surface processes. Diffusive processes, such as regolith creep, have apparently shaped gently convex summits and solifluction has dominated on higher gradient downslope segments. On the steepest, lowermost slopes imbricated blocks and boulder sheets indicate that shallow landsliding and boulder tumbling have been active in addition to solifluction. Further deposition of transported material has occurred at the concave bases of these slopes where scattered boulders are embedded in, and rest upon, a fine-matrix-rich regolith. The abundance of the fine matrix here and numerous boulders, some of non-local lithology, resting on the ground surface also indicate an additional contribution of glacial till. The Tarfalatjårro transect terminates 73 m below the summit in an autochthonous blockfield-mantled saddle and intersects only the diffusion-dominated segment. In contrast, the Alddasčorru transect terminates on the steep mass-wasting segment 278 m below the summit, whereas the Duoptečohkka transect intersects each of these segments and the solifluction-dominated segment and terminates 270 m below the summit on the mixed colluvium and till segment (Fig. 1).

Each blockfield is developed on amphibolite. Lithological variations were not observed along either of the Alddasčorru or Duoptečohkka transects except for some granitic glacial erratics. In contrast, plagioclase-porphyritic and highly schistic amphibolites were observed along the Tarfalatjårro transect, which terminates at its lower end on metapsammite. Glacial erratics also occur occasionally on Tarfalatjårro but were not observed along the profile.

The blockfields along each transect form areally continuous mantles, and bedrock outcrops are generally absent. An exception occurs on the narrow, ridge-like summit of Duoptečohkka, where bedrock is frequently exposed. The blockfield surfaces are dominated by cobbles and boulders (> 90 % area) with patches of fine matrix visible only in the centres of interspersed periglacially sorted circles (mean diameters of 1.5–2.0 m) on Alddasčorru, Tarfalatjårro, and on the upper flanks of Duoptečohkka. The Duoptečohkka summit blockfield is not periglacially sorted, and fine matrix is absent from the surface. Ventifacted boulders and loess deposits are absent from each transect.

The study area is located where the Arctic maritime climate of Norway converges with the continental climate of northern Sweden. The mean annual air temperature (MAAT) on Tarfalatjårro during 1946–1995, as inferred from records of nearby Tarfala Research Station at 1130 m a.s.l. (Fig. 1), was approximately -6 °C and mean annual precipitation (MAP) was about 500 mm (Grudd and Schneider, 1996). More recent data from a permafrost monitoring borehole on Tarfalatjårro indicate a MAAT at 2 m above the ground of -4.3 °C and mean annual ground temperatures of -2.8 and -3.0 °C, at 0.2 and 2.5 m depth respectively, over 2003–2005 (Isaksen et al., 2007). The closest meteorological station to Alddasčorru and Duoptečohkka is located at 380 m a.s.l. at the Abisko Scientific Research Station. (Fig. 1). It has recorded a MAAT of -0.9 °C and MAP of about 320 mm (Eriksson, 1982), which is a warmer and drier climate than occurs on Tarfalatjårro. Based on this MAAT we infer that MAATs are also below zero on Alddasčorru and Duoptečohkka. Permafrost is present on each of the three summits, with the monitoring borehole on Tarfalatjårro indicating a distinct warming trend and a present active layer thickness of 1.4–1.6 m (Isaksen et al., 2001, 2007). Snow covers Tarfalatjårro from about October to May, although strong winds limit the maximum snow depth to about 0.3 m (Isaksen et al., 2001). Similar temperature, snow, and permafrost conditions are expected and assumed for Alddasčorru and Duoptečohkka. Vegetation along each transect is restricted to lichens, mosses, and occasional grasses, except for the base of the Duoptečohkka transect, which is well grassed. Stable lichen-covered surface clasts indicate that, although they have occurred in the past, large-scale periglacial sorting and gelifluction processes appear to be now largely inactive. However, upfreezing of pebbles and creep and gelifluction processes over a few tens of centimetres remain active.

The northern Swedish Scandes have been repeatedly glaciated during the Quaternary, with cirque glaciation inferred to have been dominant before 2.0 million years ago (Ma), mountain ice sheets dominant between 2.0 and 0.7 Ma, and Fennoscandian ice sheets developing over the last 0.7 Ma (Kleman and Stroeven, 1997; Kleman et al., 2008). Current glaciation in the region is confined to small icecaps and small cirque and valley glaciers. During glacial periods, relatively high-altitude surfaces such as Tarfalatjårro, Alddasčorru, and Duoptečohkka were either exposed as nunataks or covered by cold-based ice sheets (Stroeven et al., 2006). The occasional erratics on Tarfalatjårro and abundant granitic erratics on Alddasčorru and the flanks of Duoptečohkka confirm former ice sheet coverage as late as 12 ka (Fabel et al., 2002; Stroeven et al., 2006). However, the presence of autochthonous blockfields and the absence of till sheets and glacial erosion features, such as striated bedrock outcrops, indicate extremely minor glacial modification of Tarfalatjårro and Alddasčorru. Clear evidence of glacial processes is also absent from Duoptečohkka. We therefore consider the presently thin autochthonous blockfield and outcropping bedrock to be attributable to slope transport processes operating across this narrow summit, although some glacial entrainment of blocks cannot be entirely discounted.

3 Methods

3.1 Field techniques

To determine the composition of blockfield regoliths, a total of 26 pits were hand excavated along the three hillslope transects during August 2004–2006: 7 pits on Alddasčorru, 10 pits on Duoptečohkka, and 9 pits on Tarfalatjårro (Fig. 1). Blockfield sections were examined in 15 of these pits, which were excavated across sorted circles, from clast-dominated rings to fine matrix-rich circle centres, or into clast-rich solifluction lobes. The pit excavated into the summit of Duoptečohkka was an exception because the thin regolith (< 0.5 m) and frequent bedrock exposures prevented periglacial sorting. The pits were excavated either until large amphibolite slabs prohibited sampling of deeper sections, the water table was intersected, or bedrock was reached. Fine matrix samples were taken from 16 blockfield pits for grain size, XRD, and SEM analyses. For replication purposes, at least three fine matrix samples were taken from each of the four surface process segments: (1) low-gradient diffusive, (2) solifluction slope, (3) steep mass-wasting, and (4) concave depositional, if and where they occur on the three transects. Segment 3 was only sampled on the Alddasčorru transect, and only one sample was analysed from segment 2 on the Alddasčorru transect. Because we previously found that only minor variations occur in fine matrix granulometry and secondary mineralogy with depth beneath the ground surface (Goodfellow et al., 2009), only one sample was analysed from each pit. An exception occurred for the Alddasčorru summit pit, from which surface, 0.16 m, and 0.60 m depth samples were processed. For comparative purposes, fine matrix samples were taken for grain size, XRD, and SEM analyses from tills covering Ruohtahakčorru (Fig. 1; 68°09′ N, 19°20′ E; 1342–1346 m a.s.l.; three samples from 0.5, 0.9, and 1.2 m depth) and Nulpotjåkka (Fig. 1; 67°48′ N, 18°01′ E; 1405 m a.s.l.; one sample from 0.9 m depth).

Two quartz clasts were collected from the summit surfaces of Duoptečohkka and Tarfalatjårro for measurements of in situ-produced ^{10}Be and ^{26}Al concentrations. Sampling was undertaken on summits to eliminate the possibility of these clasts having been transported and buried by slope processes, which would complicate estimates of regolith residence durations from measurements of ^{10}Be and ^{26}Al concentrations. This constraint, coupled with the scarcity of summit vein quartz, limited our sampling for TCN analyses to these two sites. Zero vertical mixing was assumed for the vein quartz clast (4 cm thick) sampled from the Duoptečohkka summit (Fig. 2a, b). This is because this long clast (0.19 m) resided on the surface of a thin regolith (0.3 m depth), and periglacially sorted circles were absent from this site. Because of the absence of glacial erratics from Duoptečohkka and the presence of quartz veins in these blockfields, we considered the sampled clast to be locally derived. On Tarfalatjårro, the clast (3–4 cm thick) was taken from a shattered quartz vein (~ 8 m in length) that extended ~ 8 m across the blockfield surface (Fig. 2c, d). Zero vertical mixing of the sampled clast through the regolith profile was again assumed because the quartz vein was clearly expressed at the blockfield surface, periglacially sorted circles did not intersect the quartz vein, and the fine matrix required for periglacial sorting (Ballantyne and Harris, 1994, pp. 85–96) was sparse, resulting in limited vertical and lateral sorting of clasts. While both samples were taken from autochthonous amphibolite blockfields, the narrow, high curvature summit of Duoptečohkka, which also displays frequent bedrock outcrops, contrasts with the broad, comparatively low curvature, comprehensively regolith-mantled summit of Tarfalatjårro. A higher erosion rate and shorter regolith residence duration was therefore expected for Duoptečohkka.

To correct for topographic shielding the surface geometries of the sampled blockfields and surrounding summits were measured with a clinometer and compass. Sample locations were recorded with a handheld GPS and on a 1:50 000 topographic map. Three amphibolite clasts and three fine matrix samples extracted in a cylinder of known volume were collected for regolith clast and matrix density measurements.

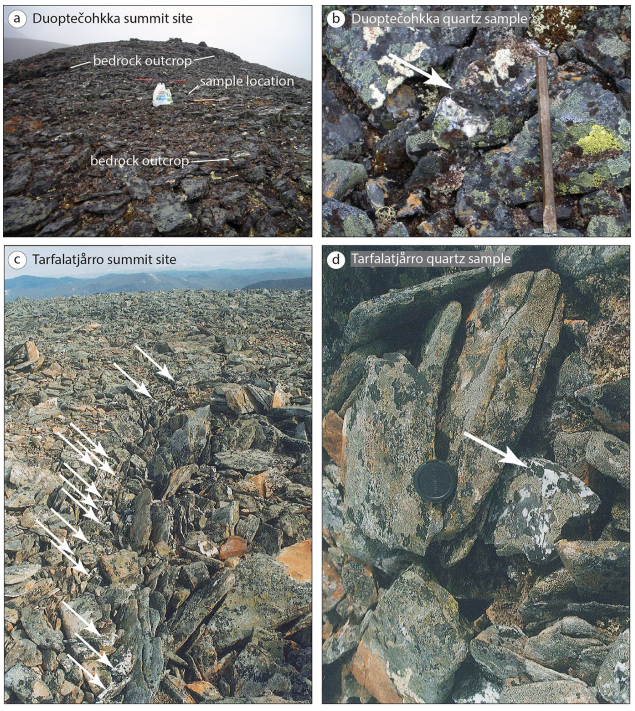

Figure 2. Sample sites for surface quartz clasts on the summits of **(a, b)** Duoptečohkka and Tarfalatjårro **(c, d)**. The quartz sampled on Duoptečohkka (arrow in **b**) was an isolated mass attached to an amphibolite block whereas the quartz clast sampled on Tarfalatjårro (arrow in **d**) was part of a frost-shattered quartz vein that extended ~ 8 m across the blockfield surface (arrows in **c**).

3.2 Fine matrix analyses

To determine the chemical weathering characteristics of blockfields, grain size, SEM, and XRD analyses were completed. Grain sizes were determined on dried samples with a Coulter LS particle size analyser. SEM analyses of chemical etching were performed on surface bulk fine matrix samples and semi-quantitative analyses of grain chemistry and mineralogy were completed according to energy dispersive spectrometer techniques (Goldstein et al., 2003). Thin sections for mineralogical interpretation of parent material were prepared from two Alddasčorru rock samples.

For XRD analysis of clay mineralogies, the $< 2\,\mu m$ size fraction of each sample was separated by settling, Mg-saturated, and purified with a ceramic filter to produce oriented samples. An initial XRD scan was performed at 2–69° 2θ with a scan speed of 0.02° $2\theta\,s^{-1}$ and a step size of 0.04° 2θ. Second and third scans were performed following ethylglycol saturation and heating of the samples to 550 °C, respectively. These scans were performed at 2–35° 2θ with a scan speed of 0.0067° $2\theta\,s^{-1}$ and a step size of 0.04° 2θ. Diffraction peaks were analysed with peak search software and manually reviewed using Brindley and Brown (1980) and Moore and Reynolds (1997).

3.3 Cosmogenic radionuclide analyses and ice sheet modelling

Concentrations of ^{10}Be and ^{26}Al in samples of vein quartz were measured to estimate erosion rates and residence durations of blockfield regoliths. Clean quartz separates were processed for cosmogenic nuclide analyses through methods adapted from Kohl and Nishiizumi (1992) and Child et al. (2000). Accelerator mass spectrometry (AMS) measurement of the Tarfalatjårro sample was completed at PRIME Lab, Purdue University, USA, and AMS measurement of the Duoptečohkka sample was completed at the SUERC AMS Laboratory, East Kilbride, UK. Measured TCN concentrations were corrected by full chemistry procedural blanks and normalized using the NIST ^{10}Be standard (SRM4325) with a ^{10}Be / ^{9}Be ratio of $(2.79 \pm 0.03) \times 10^{-11}$ and using a ^{10}Be half-life of 1.36×10^{6} a (Nishiizumi et al., 2007) and the PRIME Lab ^{26}Al standard (Z92-0222) with a nominal ^{26}Al / ^{27}Al ratio of 4.11×10^{-11} and using an ^{26}Al half-life of 7.05×10^{5} a (Nishiizumi, 2004). Errors in nuclide concentrations include the quadrature sum of analytical uncertainty calculated from AMS counting statistics and procedural errors.

Apparent exposure ages were calculated from ^{10}Be and ^{26}Al concentrations using the CRONUS-Earth exposure age calculator (version 2.2; Balco et al., 2008) assuming zero erosion and the Lal–Stone time-independent ^{10}Be production rate model (Lal, 1991; Stone, 2000). The time-independent Lal–Stone scaling was used here because we also used it for modelling regolith residence durations for reasons described below. We do though cite in our results the full age ranges given for all production rate models incorporated into the CRONUS-Earth exposure age calculator. Corrections were applied for topographic shielding (scaling factors > 0.9998) and for sample thickness using a clast density of $2.65\,g\,cm^{-3}$. Apparent exposure ages are not corrected for snow shielding because of high uncertainties, and a correction for vegetation shielding is not required. Quoted exposure age uncertainties (1σ external) include nuclide production rate uncertainties and the concentration errors described above. The apparent exposure ages for these sites are minimum durations to which the effects on nuclide production rates of surface burial by snow and glacial ice, and elevation changes attributable to glacial isostasy are subsequently added.

Regolith residence durations, incorporating periods of subaerial exposure and burial by glacial ice, of the Duoptečohkka and Tarfalatjårro summit blockfields were calculated from measured ^{10}Be concentrations accordingly (rearranged from Lal, 1991):

$$\frac{N_i}{N} = [1-\beta]\exp\{(\lambda+\alpha)t\} + \beta, \quad (1)$$

where N is nuclide concentration, with the subscript i indicating one step back in time; λ the nuclide half-life; t the time step, and where

$$\alpha = \frac{E\rho}{\Lambda}, \quad (2)$$

where E is the erosion rate ($cm\,a^{-1}$), ρ the regolith density, and Λ the attenuation mean free path, and

$$\beta = \frac{P}{N(\lambda+\alpha)}, \quad (3)$$

where P is nuclide production rate. During periods of surface burial by ice sheets, Eq. (1) is simplified to

$$\frac{N_i}{N} = \exp\{\lambda t\}. \quad (4)$$

Regolith residence durations are obtained when zero nuclide concentrations are reached.

The source code for the CRONUS-Earth exposure age calculator (version 2.2; Balco et al., 2008) was not used for calculating these regolith residence durations because of the complexities introduced by accounting for depth- and time-averaged ^{10}Be production rates. Rather, a sea-level high-latitude ($> 60°$) ^{10}Be production rate of 4.59 ± 0.28 atoms $g^{-1}\,a^{-1}$, from the Nishiizumi et al. (2007) ^{10}Be half-life of 1.36×10^{6} a, was used in these calculations. Production rates were scaled to latitude and altitude using Stone (2000) and a sea surface temperature of 5 °C. The errors in regolith residence durations attributable to our use of simplified ^{10}Be production rates are minor compared with uncertainties attributable to surface burial by snow and ice and isostatic responses to ice sheet loading and unloading.

A constant blockfield density of 2.60 g cm^{-3} was assumed based on a blockfield containing 15 % fine matrix, with a density of 2.10 g cm^{-3} (mean of three samples, $1\sigma = 0.09$), and 85 % amphibolite, with a density of 2.79 g cm^{-3} (mean of three samples, $1\sigma = 0.02$). The effects of regolith dissolution were ignored because regolith residence durations that include multiple periods of surface exposure and burial by ice sheets preclude erosion rate calculations directly from nuclide concentrations. Furthermore, chemical weathering in these blockfields is likely to be minor (Goodfellow et al., 2009). Corrections were applied for shielding and for sample thickness using an attenuation mean free path of 160 g cm^{-2} and a quartzite density of 2.65 g cm^{-3}. A correction for snow burial was also incorporated assuming 0.3 m of snow (Isaksen et al., 2007), with a density of 0.3 g cm^{-3}, for a duration of 7 months per year. The resulting annual shielding by snow of only 5.25 g cm^{-2} is assumed to be representative of all ice-free periods. Associated uncertainties are, however, unknown but, because they are high, a sensitivity analysis was performed by increasing the depth of burial from 0.30 to 0.50 m and increasing duration of burial from 7 to 10 months a year in a calculation of regolith residence duration.

To incorporate periods of surface burial by ice sheets into calculations of regolith residence durations, and to explore the effects of glacial isostasy on these calculations, we used a 3-dimensional ice-dynamical model forced by the Lisiecki and Raymo (2005) stack of global benthic δ^{18}O records and an ELRA bedrock model. Full details of the ice-dynamical model can be found in Bintanja et al. (2002, 2005). An ELRA model offers the best glacial isostasy approximation among the group of simple models, with its primary weakness being that it incorporates only one time constant (Le Meur and Huybrechts, 1996). Whereas self-gravitating visco-elastic spherical Earth models are the most accurate, they are much more complex and require greater computational power and time (Le Meur and Huybrechts, 1996). The ice sheet model was run at 40 km resolution, with a 100-year time step over the last 1.07 Ma. Although spatial resolution is coarse, using a 20 km grid provides minimal change in bedrock topography and calculations on a 50 m digital elevation model of the northern Swedish mountains produced the same mean elevations for 40×40 km squares centred on the relevant model grid points. Furthermore, the wavelength of glacial isostasy is much longer than the topographic wavelength (Le Meur and Huybrechts, 1996). Regional ice sheet thickness is subsequently more important than local ice sheet thicknesses for determining isostatic response, and a grid size of some tens of kilometres appears justified. A limitation of our models' treatment of isostasy is that it lacks an erosion component. However, the consequence of this on isostasy over successive late Quaternary glacial cycles is likely to be less important in this landscape of apparent selective linear erosion than in other alpine locations where glacial erosion was more aerially extensive. For example, Staiger et al. (2005) estimate limited net regional glacial erosion and a low glacial erosion efficiency for the Torngat Mountains in Labrador, Canada, which consist of similar lithologies to the Scandes and which were also subjected to selective linear glacial erosion during the Quaternary. Our model may also underestimate surface burial durations because smaller ice masses may have formed on summits in between the periods of regional ice sheet coverage that are captured in our model. However, ice sheet models that have the required resolution to account for the formation of these small ice masses are not run over multiple glacial cycles because of the high computational burden. Furthermore, the two summits used in our study are perhaps unlikely locations for small ice masses to form, because they are subjected to strong winds, or to persist well after larger ice masses have retreated, because of their locations on the crests of high ridges. We therefore consider our model to offer a reasonable approximation (with estimated ±20 % error margins) of ice sheet burial durations and glacial isostasy.

4 Results

4.1 Blockfield structure

Blockfield vertical sections along the Alddasčorru, Duoptečohkka, and Tarfalatjårro altitudinal transects display a number of common features (Fig. 3). Surface exposures of cobbles and boulders comprise the outer rings of periglacially sorted circles on low-gradient surfaces and delineate solifluction lobes on slopes. In addition to lichen covers, subaerially exposed clast surfaces on sorted circles display rounding through granular disintegration, which further confirms presently limited regolith mixing on low-gradient surfaces. In contrast, freshly exposed fine matrix and loose clasts indicate that some solifluction lobes remain active. In each setting, surface cobbles and boulders are underlain by a layer of gravel and larger clasts to average depths of 0.9–1.0 m beneath the ground surface. In the centres of fine matrix-rich sorted circle centres, surface layers of cobbles and boulders are usually underlain by fine matrix, granules and gravel, in which cobbles and boulders are embedded, to depths up to 0.7 m. Excavation depths generally ranged between 0.6 and 1.3 m, and the bottom of each pit typically consisted of boulders embedded in a fine matrix that ranged from damp to water saturated (Table S1 in the Supplement). The Duoptečohkka summit pit was excavated to bedrock, which was reached at only 0.30 m. None of the pits revealed soil horizons or saprolite.

Although only about 10 % of the ground surface consists of fine matrix, it appears to comprise about 10–20 % of the subsurface regolith (Table S1 in the Supplement). Surface fine matrix is most abundant on the section of the plateau into which Alddasčorru pit 4 was dug (∼ 50 % of the surface area) and in the saddle into which Tarfalatjårro pits 6–9 were dug (∼ 30 % of the surface area). Sub-surface fine matrix appears most limited on the summits of Alddasčorru and

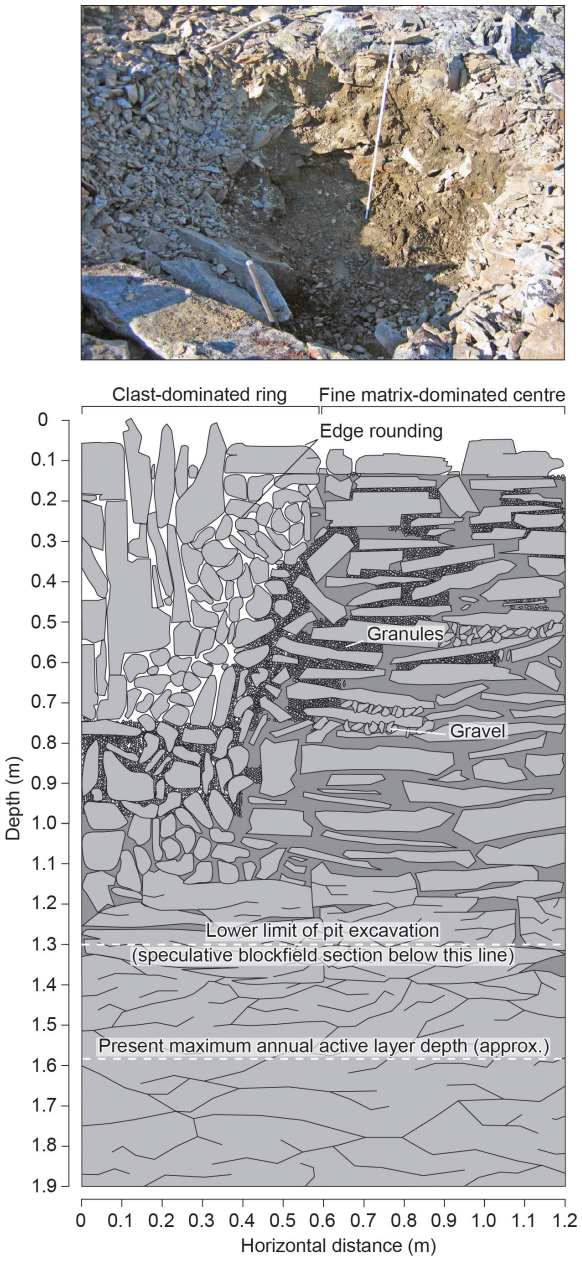

Figure 3. Representative vertical sections of autochthonous blockfields. The photograph shows an excavation across one of the sparsely distributed sorted circles developed in the summit blockfield of Tarfalatjårro, and the line drawing summarizes the general features of autochthonous blockfields in a vertical section cut across a periglacially sorted circle. The ruler in the photograph is 1 m in length. Angular cobbles and boulders are embedded in fine matrix (clay, silt, sand) in sorted circle centres. Granules and gravel accumulate between clasts distributed vertically through the section that have subhorizontally oriented long axes. Conversely, the outer ring of the sorted circle is comprised of gravel, cobbles, and boulders, whereas granules accumulate near the base of the section. Clast surfaces are sub-rounded where they are subaerially exposed. The pit bases generally intersect large rock slabs and are wet.

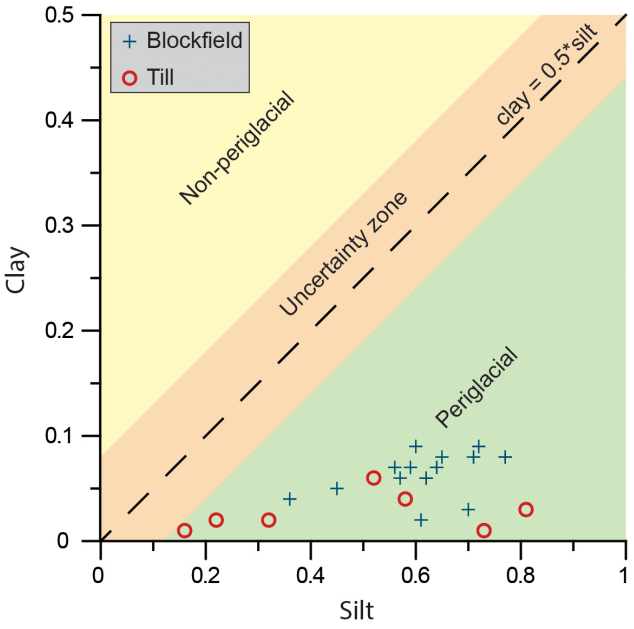

Figure 4. Quantities of clay and silt in fine matrix samples collected from blockfields (blue crosses) and till (red circles). All samples contain clay / silt ratios less than 0.5, which indicates fine matrix production under conditions that have been, at least seasonally, periglacial (Goodfellow, 2012). Fine matrix samples falling in the uncertainty zone may have been exposed to periglacial conditions during their formation (Goodfellow, 2012). All data have been divided by 65 to fit on 0–1 scales.

Tarfalatjårro (5–15 %), and in the solifluction lobes on the slope of Duoptečohkka (pits 4 and 5, 5–10 %; Table S1 in the Supplement). Here, cobbles and boulders were embedded in gravel throughout most of the subsurface, with only small accumulations of fine matrix on boulder tops or in poorly defined sorted circle centres.

In summary, blockfield sections indicate present surface stability as well as regolith sorting and transport, particularly during former periods of colder climate where blockfield-mantled surfaces also remained free of glacial ice cover. Chemical weathering rates have been insufficient to produce soil horizons or saprolite.

4.2 Fine matrix granulometry

All blockfield fine matrix samples are sandy loams (Table 1; US Department of Agriculture, 1993, p. 138). However, minor variations occur in the distribution of sand ($1\sigma = 7.5\,\%$), silt ($1\sigma = 6.9\,\%$), and clay ($1\sigma = 1.3\,\%$) according to sampling depth and the subsurface distribution of boulders, between which granules, pebbles, and gravel accumulate. Till samples vary between loamy sand, sandy loam, and silt loam, and have lower mean clay quantities (1.8 %, $1\sigma = 1.1\,\%$) than the blockfield fine matrix (4.2 %, $1\sigma = 1.3\,\%$). Although clay abundances are higher in blockfields than in till,

Table 1. Particle size distribution and secondary minerals in fine matrix from Alddasčorru, Duoptečohkka, and Tarfalatjårro transects, and from Ruohtahakčorru and Nulpotjåkka summit tills.

Transect and pit	Sample[a]	Location[b] (slope segment)	Elevation (m a.s.l.)	Depth (m)	Clay (%)	Silt (%)	Sand (%)	Clay / silt	Clay minerals[c]
Alddasčorru 1	BG-05-11	Summit (1)	1538	Surface	4.9	42.2	52.9	0.12	C, I, A, P, Q
Alddasčorru 1	BG-05-04	Summit (1)	1538	0.16	3.4	29.3	67.3	0.12	C, I, A, P, Q
Alddasčorru 1	BG-05-16	Summit (1)	1538	0.60	2.7	23.6	73.7	0.11	C, I, A, P, Q
Alddasčorru 2	BG-05-26	Slope (1)	1500	0.60	4.5	36.2	59.4	0.12	C, I, A, G?, P, Q
Alddasčorru 5	BG-05-67	Slope base (3)	1260	0.40	5.8	46.5	47.7	0.12	C, V, I, A, G, P, Q
Alddasčorru 6	BG-05-68	Slope base (3)	1260	0.40	4.1	37.0	58.8	0.11	C, V, I, A, G, P, Q
Alddasčorru 7	BG-05-69	Slope base (3)	1260	0.40	3.2	29.2	67.6	0.11	C, V, I, A, G, P, Q
Duoptečohkka 5	BG-05-64	Slope (2)	1200	0.40	4.0	40.6	55.4	0.10	C, V, I, A, P, Q
Duoptečohkka 6	BG-05-65	Slope (2)	1200	0.40	4.1	40.3	55.6	0.10	C, V, I, A, G, P, Q
Duoptečohkka 7	BG-05-66	Slope (2)	1200	0.40	4.4	38.4	57.3	0.11	C, V, I, A, G?, P, Q
Duoptečohkka 8	BG-05-70	Colluvium/till (4)	1060	0.40	1.1	14.1	84.8	0.08	C, V, I, A, P, Q
Duoptečohkka 9	BG-05-71	Colluvium/till (4)	1060	0.40	3.6	34.1	62.3	0.11	C, V, I, A, G, P, Q
Duoptečohkka 10	BG-05-72	Colluvium/till (4)	1060	0.40	1.5	20.8	77.7	0.07	C, V, I, A, G?, P, Q
Tarfalatjårro 1	BG-04-25	Summit (1)	1626	1.25	1.5	39.5	59.0	0.04	C, I, A, P, Q
Tarfalatjårro 2	BG-06-22	Summit (1)	1626	Surface	5.6	39.3	55.2	0.14	C, I, A, P, Q
Tarfalatjårro 3	BG-04-26	Summit/slope (1)	1623	0.80	2.1	45.5	52.4	0.05	C, I, A, P, Q
Tarfalatjårro 6	BG-05-83	Saddle (1)	1553	0.50	4.7	41.3	54.0	0.11	C, V, I, A, G, P, Q
Tarfalatjårro 7	BG-05-84	Saddle (1)	1553	0.20	5.3	49.9	44.8	0.11	C, V, I, A, G, P, Q
Tarfalatjårro 8	BG-05-85	Saddle (1)	1553	0.20	5.4	49.8	44.8	0.11	C, V, I, A, G, P, Q
Tarfalatjårro 9	BG-06-07	Saddle (1)	1553	0.70	5.4	46.1	48.5	0.12	C, V, I, A, G, P, Q
Ruohtahakčorru	BG-04-22	Summit till	1342	0.50	2.2	52.8	45.0	0.04	C, V, I, A, P, Q
Ruohtahakčorru	BG-04-23	Summit till	1346	0.90	0.7	10.3	89.0	0.07	C, V, I, A, P, Q
Ruohtahakčorru	BG-04-24	Summit till	1343	1.20	2.6	37.7	59.7	0.07	C, V, I, A, P, Q
Nulpotjåkka	BG-04-27	Summit till	1405	0.90	0.7	47.2	52.1	0.01	C, V, I, A, P, Q

[a] BG-06-22 and BG-06-07 are representative of eight samples from Tarfalatjårro pit 2 and seven samples from Tarfalatjårro pit 9, respectively (Goodfellow et al., 2009). [b] Slope segments are numbered as follows: (1) diffusion-dominated summit, (2) solifluction-dominated slope, (3) steep mass wasting, (4) concave depositional, where regolith comprises colluvium and till. Till is indicated by the presence of clasts of different lithologies and a high abundance of fine matrix. [c] C – chlorite; V – vermiculite; I – illite; A – amphibole; G – gibbsite (? indicates uncertain); P – plagioclase (dominant feldspar); Q – quartz.

clay comprises only 1.5 to 5.8 % of the fine matrix volume, which remains at the low end of the range (1–30 %) previously reported for other blockfields (e.g. Caine, 1968; Rea et al., 1996; Dredge, 2000; Marquette et al., 2004; Paasche et al., 2006; Table A.1 in Goodfellow, 2012). Clay / silt ratios are all ≤ 0.14 (Table 1; Fig. 4). These indicate a low intensity of chemical weathering that is typical for regolith formation under, at least seasonal, periglacial conditions (Goodfellow, 2012).

4.3 Fine matrix mineralogy

XRD analyses of the clay-sized fraction of the regolith indicate the presence of primary and secondary minerals in all samples (Table 1, Fig. 5). Primary minerals are abundant and include chlorite, amphibole, and feldspar. The presence of these minerals, along with epidote, was also confirmed using thin sections. In addition to these primary minerals, small quantities of poorly crystallized Al- and Fe-oxyhydroxides are identifiable by XRD in the Alddasčorru and Tarfalatjårro summit samples. In contrast, vermiculite, gibbsite, and larger quantities of poorly crystallized oxyhydroxides are also identifiable in concave locations, such as at the base of Alddasčorru and in the Tarfalatjårro saddle. Gibbsite generally occurs together with poorly crystallized Al- and Fe-oxyhydroxides and vermiculite. A sample from the upper slope of Alddasčorru (BG-05-26; Fig. 5b) forms a possible exception, where poorly crystallized oxyhydroxides and gibbsite appear to be the only secondary minerals present. Up to two samples from the solifluction-dominated slope segment on the Duoptečohkka transect are also gibbsite-bearing. All till samples contain poorly crystallized oxyhydroxides and vermiculite, but up to two samples of mixed colluvium and till at the base of the Duoptečohkka transect also contain gibbsite. We are unable to distinguish kaolinite according to the standard XRD techniques we used because of the ubiquitous presence of chlorite (Moore and Reynolds, 1997, p. 234). However, we believe that kaolinite may be present in our samples in small quantities. Quartz and muscovite are also commonly present. Because of the scarcity of quartz in the amphibolitic parent rock, these likely represent aeolian additions to blockfields and/or are till components.

Chemical weathering was observed on only two albite grains under SEM: one through surface etching and a second through more general disintegration (Fig. 6). It was otherwise absent, even on easily weathered minerals such as amphibolite and epidote, in addition to most albite grains. This observation of sparsely weathered silt- and sand-sized grains complements the mixed primary and secondary mineralogy of clay-sized grains. Together, they provide an overall impression of generally minor chemical weathering.

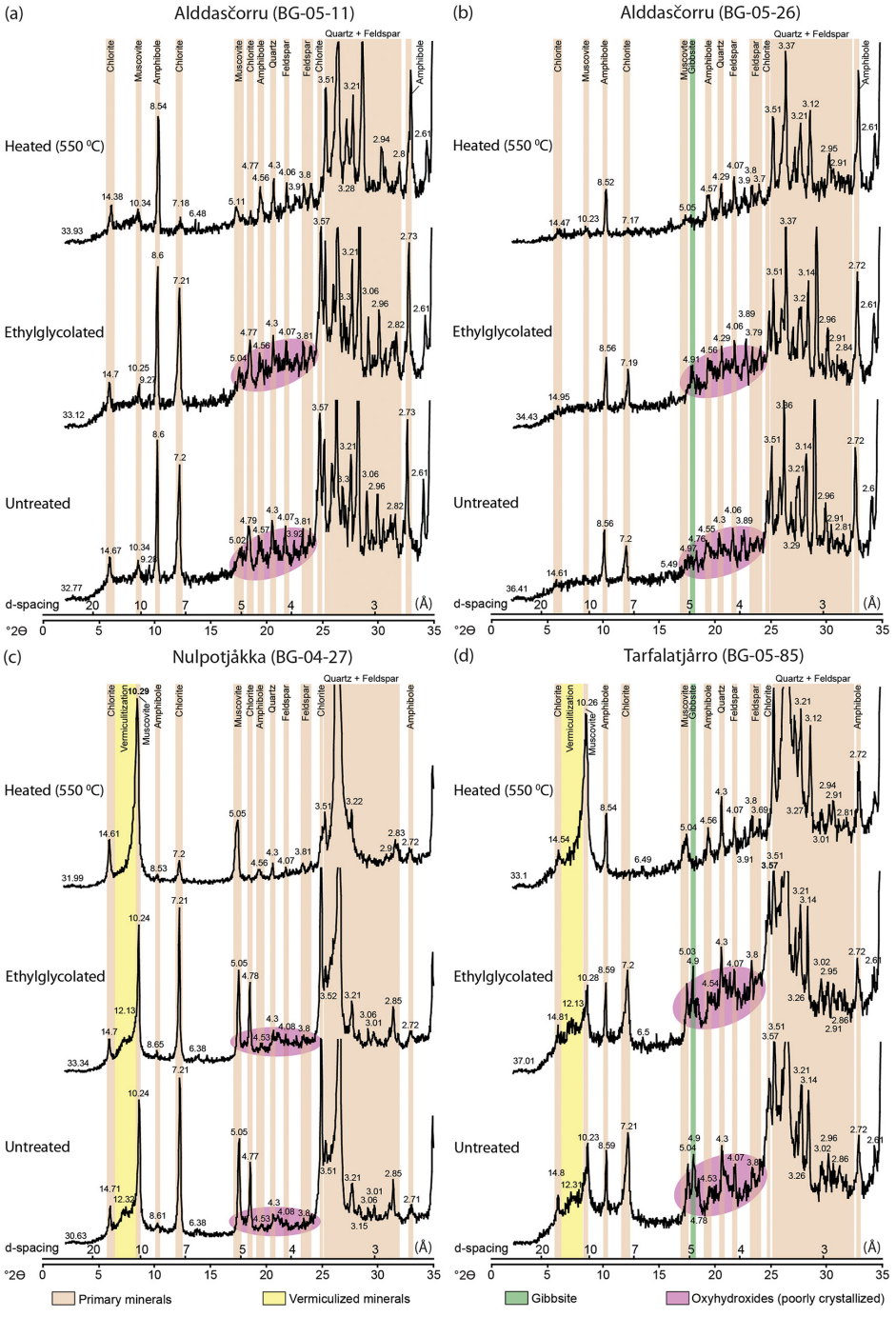

Figure 5. Four representative X-ray diffractograms of the clay-sized fraction (< 2 µm) of fine matrix samples from **(a)** Alddasčorru, **(b)** Alddasčorru, **(c)** Nulpotjåkka, and **(d)** Tarfalatjårro. For each sample three diffractograms are shown. In the bottom diffractograms the samples are untreated, in the middle diffractograms the samples are ethylglycolated, and in the top diffractograms the samples are heated to 550 °C. These diffractograms illustrate the range of minerals present (labelled) in the Alddasčorru, Duoptečohkka, and Tarfalatjårro blockfields, and in the till samples. Poorly crystallized oxyhydroxides produce a rise in the diffractogram baseline, which disappears on heating, at *d* spacings between 5 and 3.5 Å (pink-filled circles). Vermiculization of chlorite and/or mica is shown by peaks in the ∼ 10–14 Å (yellow) area that collapse to 10 Å on heating. Gibbsite is shown by peaks at 4.9 Å (green), which also collapse on heating.

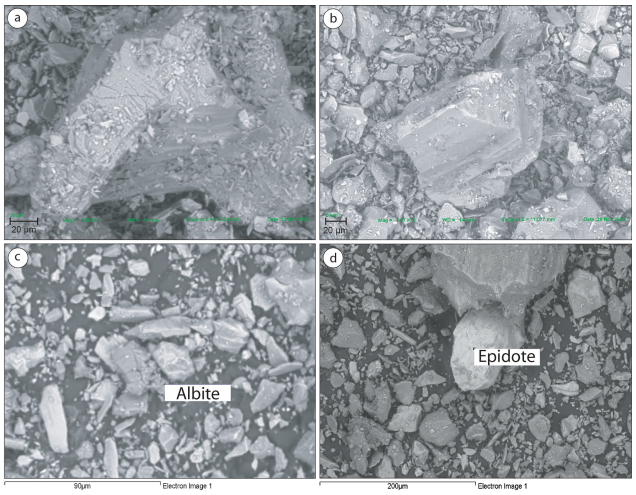

Figure 6. SEM images indicating only slight chemical weathering of fine matrix. **(a)** Albite, with a chemically etched surface; the only etched grain identified (BG-05-84, Tarfalatjårro pit 7). **(b)** Chemically unaltered amphibole, typical of all SEM images of amphibole (BG-05-26, Alddasčorru pit 2). **(c)** Disintegrating albite, possibly through chemical processes (BG-05-11, Alddasčorru pit 1). **(d)** Chemically unaltered epidote, typical of all SEM images of epidote (BG-05-04, Alddasčorru pit 1).

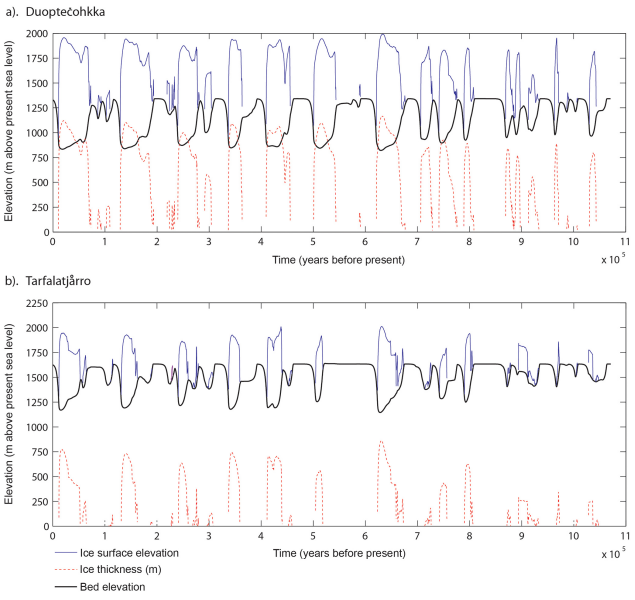

Figure 7. Modelled ice sheet surface elevation, ice thickness, and bedrock response to ice sheet loading and unloading for **(a)** Duoptečohkka and **(b)** Tarfalatjårro over the last 1.07 Ma. These data were generated using a 3-dimensional ice-dynamical model forced by the Lisiecki and Raymo (2005) stack of global benthic δ^{18}O records and the ELRA bedrock model (Bintanja et al., 2002, 2005).

In summary, XRD and SEM analyses indicate chemical weathering in blockfield and till samples, albeit in limited quantities. Samples from concave blockfield sites appear most chemically weathered, and summit blockfield fine matrix appears the least chemically weathered. Chemical weathering of till samples displays an intermediate intensity.

4.4 Regolith residence durations

Apparent ^{10}Be surface exposure durations for two surface quartzite clasts on Duoptečohkka and Tarfalatjårro are 33.5 ± 3.2 ka and 81.8 ± 7.8 ka, respectively (Table 2). These ages are based on the time-invariant spallogenic production rate model (Lal, 1991; Stone, 2000; Balco et al., 2008). For Duoptečohkka, this provides a younger age than any of the time-varying ^{10}Be spallogenic production rate models included on the CRONUS-Earth exposure age calculator (version 2.2; Balco et al., 2008). The full apparent surface exposure age range is 33.5 ± 3.2 ka to 35.6 ± 4.4 ka. For Tarfalatjårro, the apparent surface exposure age range from these production rate models is 80.4 ± 8.5 ka to 86.2 ± 10.8 ka.

The ^{26}Al / ^{10}Be ratio of 6.57 ± 0.43 for the quartz sample of the Duoptečohkka summit (Table 2) indicates no apparent burial (within error) by the Fennoscandian Ice Sheet. However, even a full exposure nuclide ratio does not exclude a complex exposure history including short intermittent periods of surface burial beneath an ice sheet. In contrast, the lower ratio of 5.92 ± 0.41 for the quartz sample of the Tarfalatjårro surface requires some previous period of burial, and, by inference, indicates periods of burial by glacial ice.

Model results for ice sheet surface elevations, ice sheet thicknesses, and glacial isostasy over multiple glacial cycles indicate that the Duoptečohkka and Tarfalatjårro summits have been repeatedly covered by ice sheets (Fig. 7). According to the model, thicker ice has formed over Duoptečohkka (a maximum of 1595 m compared with 1150 m for Tarfalatjårro) and burial durations have been longer on this summit. These data are consistent with what might be expected for the lower elevation of Duoptečohkka (1336 m a.s.l. versus 1626 m a.s.l. for Tarfalatjårro). However, they seemingly contrast with inferences from the ^{26}Al / ^{10}Be ratio for Duoptečohkka (Table 2) of either no glacial burial of this summit or surface burial during short periods relative to intermittent full-exposure durations. The thickness and duration of ice cover may therefore be overestimated in our model, and a comparison with data from other models supports this possibility. Firstly, ice sheet thicknesses produced by our model are either similar to those indicated for our study areas by other ice sheet models (Fjeldskaar et al., 2000; Milne et al., 2004; Peltier, 2004; Steffen and Kauffman, 2005) or exceed them (Peltier, 1994; Kauffman et al., 2000; Lambeck et al., 2006; Steffen et al., 2006; Charbit et al., 2007). Secondly, the magnitude of isostatic rebound following the last glaciation is 497 m for Duoptečohkka and 457 m for Tarfalatjårro. These values exceed those indicated by the isostatic rebound

Table 2. Cosmogenic nuclide data, apparent exposure ages, and nuclide ratios.

Sample[a]	Location (° N/° E)	Elevation (m a.s.l.)	Thickness[b] (cm)	Shielding factor	Quartz (g)	Be carrier (mg)	$^{10}Be/^{9}Be$[c] ($\times10^{-13}$)	$[^{10}Be]$[c,d,e,f] (10^6 atoms g^{-1})	Al carrier (mg)	$^{26}Al/^{27}Al$[c] ($\times10^{-13}$)	$[^{26}Al]$[c,f,g,h] (10^6 atoms g^{-1})	^{10}Be apparent age[c,i,j] (ka)		^{26}Al apparent age[c,i,j] (ka)		$^{26}Al/^{10}Be$[c] ratio
												Age $\pm 1\sigma$ (int)	$\pm1\sigma$ (ext)	Age $\pm 1\sigma$ (int)	$\pm1\sigma$ (ext)	
Duo 1	68.42/19.37	1330	3	1.0000	41.8211	0.3094	11.40 ± 0.30	0.51 ± 0.02	0.7222	50.10 ± 1.05	3.52 ± 0.19	33.5 ± 1.2	± 3.2	32.7 ± 1.8	± 3.4	6.57 ± 0.43
Tar 1	67.61/18.52	1626	4	0.9998	54.2814	0.2741	44.70 ± 1.20	1.55 ± 0.05	0.9028	170.00 ± 6.00	9.59 ± 0.59	81.8 ± 2.8	± 7.8	72.6 ± 4.6	± 8.0	5.92 ± 0.41

[a] Duo 1 = surface sample from Duoptečohkka pit 1; Tar 1 = surface sample from Tarfalatjårro pit 1. [b] A quartzite density of 2.65 g cm^{-3} was used for thickness corrections. [c] Uncertainties are reported at the 1σ confidence level. [d] Measured ^{10}Be concentrations were normalized to NIST SRM 4325, with a $^{10}Be/^{9}Be$ ratio of $2.79 \pm 0.03 \times 10^{-11}$ and using a ^{10}Be half-life of 1.36×10^6 a (Nishiizumi et al., 2007). [e] Blank values of 11 5436 ± 37 556 ^{10}Be atoms ($^{10}Be/^{9}Be = 6.6 \times 10^{-15} \pm 1.6 \times 10^{-15}$) and 56 776 ± 39 917 ^{10}Be atoms ($^{10}Be/^{9}Be = 4.1 \times 10^{-15} \pm 2.0 \times 10^{-15}$) were used to correct for background in Duoptečohkka 1 and Tarfalatjårro 1, respectively. [f] Propagated uncertainties include error in the blank, carrier mass (1%), and counting statistics. [g] Measured ^{26}Al concentrations were normalized to PRIME standard Z92-0222 with a nominal $^{26}Al/^{27}Al$ ratio of 4.11×10^{-11} and using an ^{26}Al half-life of 7.05×10^5 a (Nishiizumi, 2004). [h] Blank values of 337 056 ± 99 378 ^{26}Al atoms ($^{26}Al/^{27}Al = 11.4 \times 10^{-15} \pm 3.3 \times 10^{-15}$) and 183701 ± 275552 ^{26}Al atoms ($^{26}Al/^{27}Al = 6.0 \times 10^{-15} \pm 9.0 \times 10^{-15}$) were used to correct for background in Duoptečohkka 1 and Tarfalatjårro 1, respectively. [i] Apparent exposure ages were calculated using the CRONUS-Earth calculator (version 2.2; Balco et al., 2008). Constant (time-invariant) ^{10}Be and ^{26}Al spallogenic production rate models (Lal, 1991; Stone, 2000) were used. Muogenic production was also incorporated into the production rate models giving total ^{10}Be production rates of 16.138 atoms g^{-1} a^{-1} for Duoptečohkka 1 and 20.196 atoms g^{-1} a^{-1} for Tarfalatjårro 1. Total ^{26}Al production rates are 109.368 atoms g^{-1} a^{-1} for Duoptečohkka 1 and 136.788 atoms g^{-1} a^{-1} for Tarfalatjårro 1. [j] (int) – internal (analytical) uncertainties; (ext) – propagated external uncertainties (Balco et al., 2008).

map in the National Atlas of Sweden (Fredén, 2002, p. 101) by 150–250 m, which again indicates a possible overestimation of ice sheet thicknesses and durations of ice coverage by our model. The key consequences of this for our subsequent analysis of regolith residence durations are that the lengths of the ice-free periods during which cosmogenic nuclides accumulate are likely underestimated, whereas nuclide decay periods during ice sheet burial are likely overestimated. If nuclides have accumulated in surface regolith more quickly than provided for in our model and nuclide decay has been less, inferred maximum erosion rates will be underestimated and regolith residence durations, for a given erosion rate, will be overestimated in our analyses. We consider the regolith residence duration calculations to remain valid for our purposes, however, because we are interested in an order of magnitude question (i.e. whether or not regolith residence durations are confined to the late Quaternary) and to be conservative in our interpretations prefer to err on the side of overestimating regolith residence durations.

Modelled regolith residence durations for Duoptečohkka and Tarfalatjårro are shown in Fig. 8. Steps in these regolith residence duration curves indicate periods of surface burial by glacial ice. The timing of these steps in each modelled scenario varies according to erosion rate and durations of surface burial by glacial ice. The primary model output, which considers the effects of both ice sheet burial and bedrock isostasy on cosmogenic nuclide accumulation (labelled "burial and isostasy"), indicates a maximum surface erosion rate of $\sim 16.2\,mm\,ka^{-1}$ for Duoptečohkka and $\sim 6.7\,mm\,ka^{-1}$ for Tarfalatjårro. As maximum surface erosion rates are asymptotically approached, maximum surface ages become infinite. However, the regolith residence durations of Duoptečohkka and Tarfalatjårro become asymptotic above cut-off values of ∼ 380 and ∼ 490 ka before present, respectively. This indicates that the late Quaternary has likely offered sufficient time for the present regolith mantles on both summits to gain their respective ^{10}Be inventories.

Four additional regolith residence duration scenarios help define the sensitivity of derived maximum erosion rates to durations of surface burial by snow and glacial ice and to the magnitude of glacial isostasy (Fig. 8). As expected, maximum erosion rates are highest in the absence of former glaciation ("0 burial, 0 isostasy" lines in Fig. 8). These rates are $\sim 18.2\,mm\,ka^{-1}$ for Duoptečohkka and $\sim 7.3\,mm\,ka^{-1}$ for Tarfalatjårro. Accordingly, regolith residence durations for these simple exposure conditions are also lowest for this scenario. These "simple exposure" ages are ∼ 34–170 ka for Duoptečohkka and ∼ 82–375 ka for Tarfalatjårro for the range of erosion rates up to where the ages become asymptotic (Table 2; Fig. 8).

When intermittent surface burial by glacial ice is introduced, maximum erosion rates decrease to $\sim 17.5\,mm\,ka^{-1}$ and $\sim 7.1\,mm\,ka^{-1}$ for Duoptečohkka and Tarfalatjårro, respectively ("burial, 0 isostasy" lines in Fig. 8). Regolith residence durations also increase for a given erosion rate up to the erosion rate where the ages become asymptotic. These ages vary from 110 to ∼ 370 ka and 166 to ∼ 450 ka for Duoptečohkka and Tarfalatjårro, respectively.

Increasing by 10 % the duration of each period of surface burial by glacial ice has negligible impact on maximum erosion rates for either summit ("10 % more burial, isostasy" in Fig. 8). However, long burial periods are reached on Duoptečohkka at lower surface erosion rates than otherwise occur, resulting in longer regolith residence durations at these erosion rates. For example, at an erosion rate of $8\,mm\,ka^{-1}$, the regolith residence duration on Duoptečohkka increases from 123 to 199 ka. A similar effect is induced by increasing the duration of snow cover from 7 to 10 months a year and the depth of snow from 30 to 50 cm ("burial, isostasy, more snow" lines in Fig. 8). Increasing the duration and depth of snow cover decreases maximum erosion rates. These values are now $\sim 15.7\,mm\,ka^{-1}$ for Duoptečohkka and $\sim 6.3\,mm\,ka^{-1}$ for Tarfalatjårro.

In summary, the summits of both Duoptečohkka and Tarfalatjårro appear to have been repeatedly inundated by glacial ice over the past 1.07 Ma. The durations of burial and depths of glacial isostatic depression have had notable impacts on regolith residence durations for each summit. It remains likely, however, that the residence durations of regolith mantles on both summits are confined to the late Quaternary. Modelled maximum erosion rates are $\sim 16.2\,mm\,ka^{-1}$ and $\sim 6.7\,mm\,ka^{-1}$ for Duoptečohkka and Tarfalatjårro, respectively.

5 Discussion

Minimal chemical weathering of blockfields in the northern Swedish mountains is indicated by the following fine-matrix characteristics: clay / silt ratios ≤ 0.14 in all samples ($n = 16$), the presence of mixed primary and secondary minerals

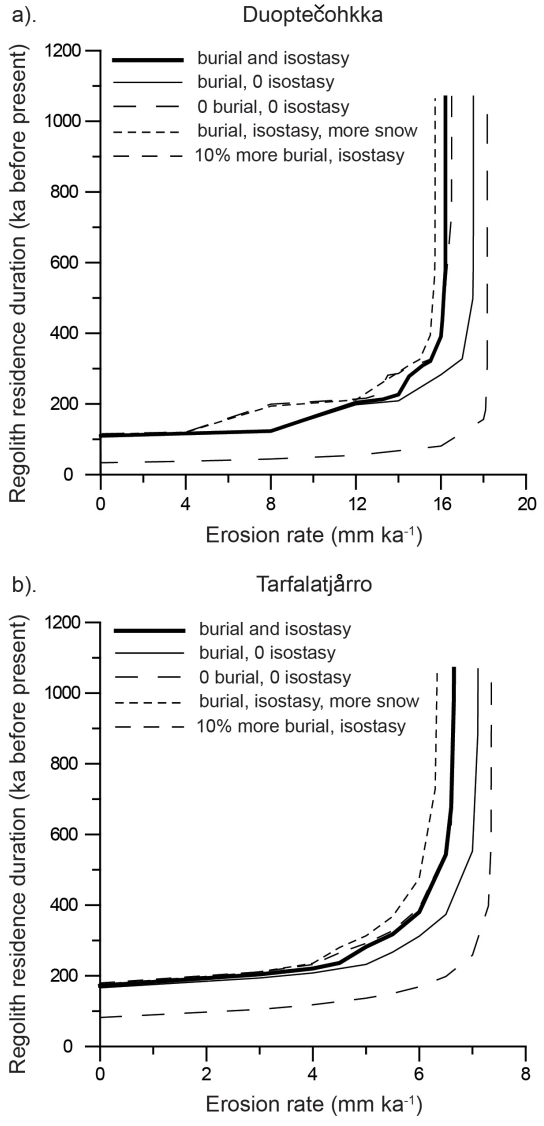

Figure 8. Regolith residence durations for **(a)** Duoptečohkka and **(b)** Tarfalatjårro plotted against surface erosion rates. These are modelled using ^{10}Be concentrations in regolith surface quartz clasts and incorporate periods of burial by ice sheets and changes in ^{10}Be production rates attributable to glacial isostasy. Seasonal burial of ground surfaces by 30 cm of snow for 7 months of the year is included. Five different scenarios were modelled: (i) ice sheet burial duration and glacial isostasy (marked "burial and isostasy" in the plots), which is our primary model output; (ii) isostasy is removed ("burial, 0 isostasy"); (iii) a simple surface exposure history, from which burial and glacial isostasy are excluded ("0 burial, 0 isostasy"); (iv) the first scenario is replicated, but snow depth and snow cover duration are increased to 50 cm and 10 months of the year, respectively ("burial, isostasy, more snow"); (v) each burial period is extended by 10 % and exposure periods commensurately shortened ("10 % more burial, isostasy").

in clay-sized regolith ($n = 16$), and a scarcity of chemically etched grains in bulk fine matrix (Table 1; Figs. 2–5). In addition, soil horizons and saprolite are absent from all blockfield sections (Table S1 in the Supplement). These findings support those from Goodfellow et al. (2009) and their model of blockfield formation, primarily through physical weathering processes. Conversely, the data do not support blockfield initiation through intense chemical weathering under a warm, non-periglacial climate.

Chemical weathering intensity, although generally low, varies predictably along hillslope transects. Convex summit areas are the least chemically weathered, as indicated by the absence of well-crystallized secondary minerals (Table 1). This is possibly because these areas are drier (Table S1 in the Supplement) or because fine matrix may not be resident on summits long enough, before being transported downslope, for secondary minerals to become well-crystallized. Concave locations, such as at the Alddasčorru slope base and the Tarfalatjårro saddle, exhibit the highest chemical weathering intensity, as indicated by the formation of vermiculite and gibbsite. This may be attributable to longer residence durations within the blockfields of fine matrix that has been transported downslope, wetter conditions, and/or changes in bedrock mineralogy (Table S1 in the Supplement). The relative paucity of summit fine matrix (Table S1 in the Supplement), which also displays lowest chemical weathering intensity (Table 1; Fig. 5), might therefore indicate erosion through, for example, surface creep and subsurface water flow. Altitudinal differences along the transects are generally insufficient for weathering variations to be clearly related to temperature changes, particularly along the 73 m Tarfalatjårro transect (Fig. 1). However, a slightly milder temperature regime and an extensive grass cover may enhance chemical weathering of the colluvium–till mixture at the base of the Duoptečohkka transect (270 m below the summit), which contains vermiculized minerals and gibbsite (Table 1). Secondary mineral assemblages are consistent with contemporary climatic conditions and hillslope position, rather than indicating palaeoregoliths.

The presence of gibbsite in some fine matrix samples does not indicate a Neogene deep-weathering origin of blockfields. Although it is an end product of chemical weathering and can be abundant in intensely weathered regoliths, formation of limited quantities of gibbsite is apparently also favoured by the generally low temperatures and spatially and temporally variable hydrologic conditions that occur in alpine regoliths. The spatial distribution of gibbsite in the blockfields of the northern Swedish Scandes indicates that its precipitation may be favoured by wetter regolith conditions found, for example, in concave locations (Table 1). Seasonally abundant liquid water may result in some leaching along spatially discrete flow paths in these blockfield regoliths (Meunier et al., 2007; Goodfellow, 2012). Together with low temperatures, which inhibit chemical reactions, this may maintain the low concentrations of H_4SiO_4 along these

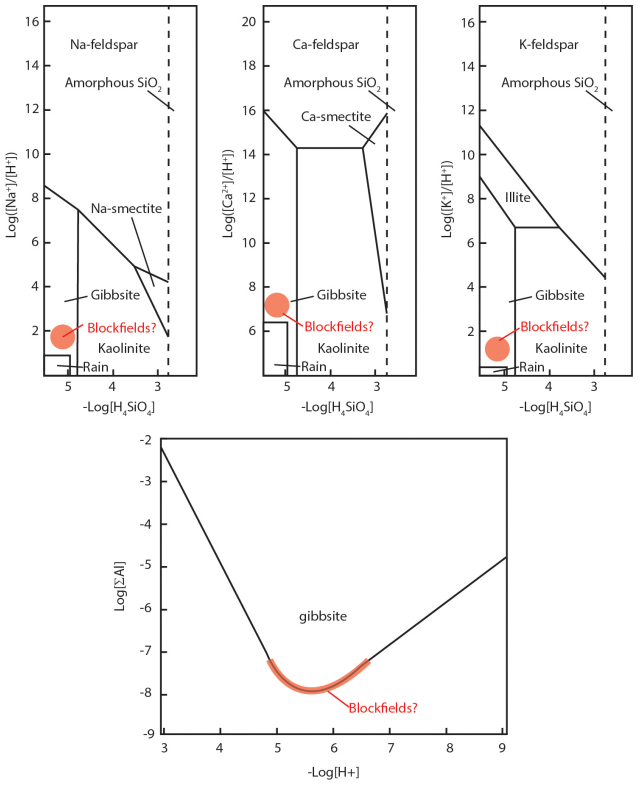

Figure 9. Thermodynamic stability relations between feldspars, secondary minerals, and weathering solutions (top panels) and the relationship between gibbsite solubility and the pH of regolith water (bottom panel). Relatively low Na^+ Ca^{2+}, and K^+ abundances and high H^+ abundances favour secondary mineral formation. Solute concentrations are usually most favourable to kaolinite precipitation, but gibbsite forms where regolith waters have very dilute silica concentrations, similar to rainwater (adapted from Stumm and Morgan, 1981, p. 547, and Nesbitt and Young, 1984, p. 1524, with permission of Wiley and Elsevier, respectively). Gibbsite is least soluble where pH is 5–6, and its solubility increases as pH is elevated or lowered from this value (adapted from Wesolowski and Palmer, 1994). It is expected that these key conditions of low silica concentration and slight acidity occur in Arctic–alpine blockfields, which favours gibbsite precipitation in these regoliths.

flow paths that are favourable to the precipitation of gibbsite rather than kaolinite (Fig. 9; Nesbitt and Young, 1984). Gibbsite may persist in blockfields because of the general absence of macro-vegetation and associated organic acids. This permits porewaters to remain slightly acidic, under which conditions gibbsite is least soluble (Fig. 9; Reynolds, 1971; May et al., 1979; Gardner, 1992; Wesolowski and Palmer, 1994). Marquette et al. (2004) measured a mean pH of 5.7 in alpine blockfield porewaters, which coincides with minimum gibbsite solubility (Fig. 9). As expected, gibbsite is present in those blockfields (located in NE Canada). The low temperature constraint on weathering reactions may further ensure the persistence of gibbsite rather than it being converted to kaolinite through resilication (Watanabe et al., 2010). The presence of gibbsite in alpine regoliths is well documented (Green and Eden, 1971; Reynolds, 1971; McKeague et al., 1983; Bain et al., 1994; Rea et al., 1996; Dahlgren et al., 1997; Ballantyne, 1998; Ballantyne et al., 1998; Burkins et al., 1999; Marquette et al., 2004; Paasche et al., 2006; Watanabe et al., 2010; Hopkinson and Ballantyne, 2014), and it should not be used to indicate that regoliths have necessarily originated under a warmer-than-present pre-Quaternary climate.

Late Quaternary surface erosion rates on the Duoptečohkka and Tarfalatjårro summits are low. These values are 16.2 mm ka^{-1} (with a range of 15.7–18.2 mm ka^{-1} for the modelled scenarios) and 6.7 mm ka^{-1} (with a range of 6.3–7.3 mm ka^{-1} for the modelled scenarios) for Duoptečohkka and Tarfalatjårro, respectively (Fig. 8). The higher erosion rate for Duoptečohkka likely reflects enhanced regolith transport across the narrow, steeply sided, summit ridgeline. This is perhaps indicated by a patchy regolith only a few tens of centimetres thick and by older bedrock apparent surface exposure durations from relict non-glacial surfaces on a nearby part of Alddasčorru (1380 m a.s.l.) and Olmáčohkka (1355 m a.s.l.) of 42.1 ± 2.5 and 58.2 ± 3.5 ka (analytical errors only), respectively (Fig. 1; Fabel et al., 2002; Stroeven et al., 2006). The lower erosion rate for the broad, low gradient summit of Tarfalatjårro likely approaches the minimum limit for blockfield-mantled surfaces in this landscape, and is based on an apparent exposure duration which is similar to one derived from bedrock on nearby Dárfalcohkka (1790 m a.s.l.) of 72.6 ± 4.4 ka (analytical error only; Fig. 1; Stroeven et al., 2006). Blockfields therefore appear to represent end-stage landforms (Granger et al., 2001; Hättestrand and Stroeven, 2002; Boelhouwers, 2004) that effectively armour low-gradient surfaces, making them resistant to erosion and limiting further modification of surface morphology and regolith composition and thickness.

While average erosion rates of blockfield-mantled summits are low, they are of sufficient magnitude to remove $\sim$ 1–2 m thick regolith profiles within a late Quaternary time frame, even accounting for periods of surface protection during burial by cold-based glacial ice (Figs. 7–8). If our conclusion that blockfields represent end-stage landforms resistant to further modification is correct, then it is reasonable to also assume steady-state conditions, where the rate of regolith production through weathering processes equals the erosion rate. Together, erosion and regolith production rates of 6–18 mm ka^{-1} and geochemical features including mixtures of primary and secondary minerals in clay-sized regolith, low clay / silt ratios, and sparsely weathered primary mineral grains are consistent with blockfield formation under, at least, seasonal periglacial conditions during the late Quaternary.

The contrast between low rates of regolith production and erosion in blockfield mantles and the apparent comprehensive removal of presumably more-intensely weathered

Neogene regoliths from the northern Swedish Scandes is intriguing. One possible explanation for this contrast is that erosion rates may have greatly outpaced regolith production rates during the onset of cold Quaternary climatic conditions. This is because protective vegetative covers may have been lost during this period, and the intensity of periglaciation may have greatly increased. In Canadian Arctic plateau landscapes similar to the Scandinavian Mountains, there is evidence of extensive removal of Neogene regolith during the early Quaternary (Refsnider and Miller, 2013). Different conditions, including perhaps less intense Quaternary periglaciation, have allowed the persistence of pre-Quaternary saprolite remnants in low-altitude locations in Scandinavia (Lidmar-Bergström, 1997). While our data indicate residence durations of present regoliths, they do not address the question of how long blockfields have mantled portions of the Scandes. Furthermore, they provide only minimum estimates of the ages of surfaces on which the blockfields reside. However, because the Plio-Pleistocene transition may have been a period of marked disequilibrium in surface processes, blockfields perhaps formed during or after this period.

Our data indicate relative stability of blockfield-mantled summits during the late Quaternary. They are therefore incompatible with the operation on these summits of a periglacial or glacial "buzz saw" during this period. However, they discount neither a "buzz saw" effect on topographic relief during earlier periods, as has been previously suggested (Pedersen and Egholm, 2013), nor more rapid late Quaternary erosion rates on higher-gradient slopes. Field observations of extensive solifluction on slopes coupled with a marked absence of remnant glacial erosion features across a range of spatial scales, such as striae, roches moutonnées, rock drumlins, whalebacks, and crag and tails, are compatible with lowering of relief on blockfield-mantled surfaces through periglacial, rather than glacial, processes. We also speculate that formation of autochthonous blockfields on glacially eroded bedrock surfaces would be greatly inhibited. This is because of low water retention against, and low infiltration into, subaerially exposed, glacially polished, and generally convex rock surfaces (André, 2002; Ericson, 2004; Hall and Phillips, 2006), which are essential for regolith production through chemical processes and frost action (Walder and Hallet, 1985; Anderson, 1998; Whalley et al., 2004; Dixon and Thorn, 2005; Goodfellow et al., 2009). Glacially scoured bedrock surfaces might therefore be resistant to regolith formation over timescales of 10^5–10^6 years (or longer), and the sum of ice-free periods during the Quaternary may have been insufficient for weathering and erosive processes to have completely removed evidence of any early Quaternary glacial erosion from the landscape. We do consider though that (early) Quaternary periglacial processes may have modified presently blockfield-mantled surfaces to a greater extent than can be easily recognized (Anderson, 2002; Goodfellow, 2007; Berthling and Etzelmuller, 2011).

The utility of blockfield-mantled surfaces as markers from which to estimate Quaternary glacial erosion volumes in surrounding landscape elements remains uncertain. This is because potentially large spatial variations in rates of non-glacial erosion on blockfield-mantled topography may have lowered local relief and altered the topography from its preglacial configuration (Anderson, 2002; Goodfellow, 2007). In addition, presently blockfield-mantled surfaces may have undergone vertical erosion exceeding some tens of metres, as well as topographic reconfiguration, during the Plio-Pleistocene transition to a colder climate. Confirmation that these slowly eroding landforms persist over multiple glacial–interglacial cycles does, however, further demonstrate the utility of these landforms as key markers of nunataks and/or cold-based ice coverage during (at least) late Quaternary glacial periods.

6 Conclusions

Blockfields on three mountains in the northern Swedish Scandes were examined, and none of them appear to be remnants of thick, intensely weathered Neogene weathering profiles, which has been the prevailing opinion for these regoliths. Minor chemical weathering is indicated in each of the three examined blockfields, with predictable differences according to slope position. Average erosion rates of ~ 16.2 and $\sim 6.7\,\mathrm{mm\,ka^{-1}}$ are calculated for two blockfield-mantled summits, from concentrations of in situ-produced cosmogenic ^{10}Be in surface quartz clasts that were inferred not to have been vertically mixed through the regolith. Although low, these erosion rates are of sufficiently high magnitude to remove present blockfield mantles, which appear to be commonly $< \sim 2$ m thick, within a late Quaternary time frame. This finding remains valid even when accounting for temporal variations in ^{10}Be production rates attributable to glacial isostasy and burial of ground surfaces by snow and cold-based glacial ice. Blockfield mantles appear to be replenished by regolith formation through, primarily physical, weathering processes that operated during the Quaternary.

The persistence of autochthonous blockfields over multiple glacial–interglacial cycles confirms their importance as key markers of surfaces that were not glacially eroded through, at least, the late Quaternary. However, presently blockfield-mantled surfaces may undergo potentially large spatial variations in erosion rates, and their regolith mantles may have been comprehensively eroded during the late Pliocene and early Pleistocene. Their role as markers by which to estimate glacial erosion volumes in surrounding landscape elements therefore remains uncertain.

The Supplement related to this article is available online at doi:10.5194/esurf-2-383-2014-supplement.

Acknowledgements. We thank Ulf Jonsell, Ben Kirk, Damian Waldron, Mark Wareing, and staff at the Tarfala Research Station and Abisko Scientific Research Station for field support, Ann E. Karlsen and Wieslawa Koziel (Geological Survey of Norway, Trondheim) for completing the grain size and XRD analyses, Bjørn Willemoes-Wissing (Geological Survey of Norway, Trondheim) for assisting with SEM, Maria Miguens-Rodriguez (SUERC, East Kilbride) for guiding Goodfellow through sample preparation for AMS, and Stewart Freeman for running AMS on sample "Duo 1". Henriette Linge, an anonymous reviewer, and journal editor David Egholm are thanked for insightful comments that improved the manuscript. John Gosse, three anonymous journal reviewers and an associate editor are also thanked for helpful comments on an earlier version. The Swedish Society for Anthropology and Geography Andréefonden, Axel Lagrelius' Fond, Hans and Lillemor Ahlmanns Fond, C. F. Liljevalchs Fond, Carl Mannerfelts Fond, and Lars Hiertas minne provided funding to Goodfellow, and Swedish Research Council grants 621-2001-2331 and 621-2005-4972, and a PRIME Lab SEED grant provided funding to Stroeven. Figure 9 is adapted from p. 547 in Stumm, W., Morgan, J. J., 1981, Aquatic Chemistry, 2nd Edn., John Wiley and Sons, New York, and from Fig. 1 in Nesbitt, H. W., Young, G. M., 1984, Prediction of some weathering trends of plutonic and volcanic rocks based on thermodynamic and kinetic considerations, Geochimica et Cosmochimica Acta 48, 1523–1534, with permission of Wiley and Elsevier, respectively.

Edited by: D. Lundbek Egholm

References

Anderson, R. S.: Near-surface thermal profiles in alpine bedrock: implications for the frost-weathering of rock, Arct. Alpine Res., 30, 362–372, 1998.

Anderson, R. S.: Modeling the tor-dotted crests, bedrock edges, and parabolic profiles of high alpine surfaces of the Wind River Range, Wyoming, Geomorphol., 46, 35–58, 2002.

André, M. F.: Rates of postglacial rock weathering on glacially scoured outcrops (Abisko-Riksgränsen area, 68° N), Geograf. Annal., 84A, 139–150, 2002.

André, M. F.: Do periglacial landscapes evolve under periglacial conditions?, Geomorphology, 52, 149–1164, 2003.

André, M. F., Hall, K., Bertran, P., and Arocena, J.: Stone runs in the Falkland Islands: Periglacial or tropical?, Geomorphol., 95, 524–543, 2008.

Bain, D. C., Mellor, A., Wilson, M. J., and Duthie, D. M. L.: Chemical and mineralogical weathering rates and processes in an upland granitic till catchment in Scotland. Water, Air Soil Pollut., 73, 11–27, 1994.

Balco, G., Stone, J. O., Lifton, N. A., and Dunai, T. J.: A complete and easily accessible means of calculating surface exposure ages or erosion rates from ^{10}Be and ^{26}Al measurements, Quaternary Geochronol., 3, 174–195, 2008.

Ballantyne, C. K.: Age and significance of mountain-top detritus, Permafrost Perigl. Process., 9, 327–345, 1998.

Ballantyne, C. K.: A general model of autochthonous blockfield evolution, Permafrost Perigl. Process. 21, 289–300, 2010.

Ballantyne, C. K. and Harris, C.: The Periglaciation of Great Britain, Cambridge University Press, Cambridge, 1994.

Ballantyne, C. K., McCarroll, D., Nesje, A., Dahl, S. O., and Stone, J. O.: The last ice sheet in north-west Scotland: Reconstruction and implications, Quaternary Sci. Rev. 17, 1149–1184, 1998.

Berthling, I. and Etzelmüller, B.: The concept of cryo-conditioning in landscape evolution, Quaternary Res., 75, 378–384, 2011.

Bierman, P. R., Marsella, K. A., Patterson, C., Davis, P. T., and Caffee, M.: Mid-Pleistocene cosmogenic minimum-age limits for pre-Wisconsinan glacial surfaces in southwestern Minnesota and southern Baffin Island: a multiple nuclide approach, Geomorphology, 27, 25–39, 1999.

Bintanja, R., van de Wal, R. S. W., and Oerlemans, J.: Global ice volume variations through the last glacial cycle simulated by a 3-D ice-dynamical model, Quaternary Int., 95–96, 11–23, 2002.

Bintanja, R., van de Wal, R. S. W., and Oerlemans, J.: Modelled atmospheric temperatures and global sea levels over the past million years, Nature, 437, 125–128, 2005.

Boelhouwers, J. C.: New perspectives on autochthonous blockfield development, Polar Geogr., 28, 133–146, 2004.

Boelhouwers, J., Holness, S. Meiklejohn, I., and Sumner, P.: Observations on a blockstream in the vicinity of Sani Pass, Lesotho Highlands, southern Africa, Permafrost Perigl. Process., 13, 251–257, 2002.

Brindley, G. W. and Brown, G.: Crystal Structures of Clay Minerals and their X-ray Identification, Mineralogical Society, London, 495 pp., 1980.

Briner, J. P., Miller, G. H., Davis, P. T., Bierman, P. R., and Caffee, M.: Last Glacial Maximum ice sheet dynamics in Arctic Canada inferred from young erratics perched on ancient tors, Quaternary Sci. Rev., 22, 437–444, 2003.

Burkins, D. L., Blum, J. D., Brown, K., Reynolds, R. C., and Erel, Y.: Chemistry and mineralogy of a granitic, glacial soil chronosequence, Sierra Nevada Mountains, California, Chem. Geol., 162, 1–14, 1999.

Caine, N.: The Blockfields of Northeastern Tasmania. Publication G/6, Department of Geography, Research School of Pacific Studies, The Australian National University, Canberra, 127 pp., 1968.

Charbit, S., Ritz, C., Philippon, G., Peyaud, V., and Kageyama, M.: Numerical reconstructions of the Northern Hemisphere ice sheets through the last glacial-interglacial cycle, Clim. Past, 3, 15–37, doi:10.5194/cp-3-15-2007, 2007.

Child, D., Elliott, G., Mifsud, C., Smith, A. M., and Fink, D.: Sample processing for earth science studies at ANTARES. Nuclear Instruments and Methods in Physics Research Section B, Beam Interactions with Materials and Atoms, 172, 856–860, 2000.

Clapperton, C. M.: Further observations on the stone runs of the Falkland Islands, Biuletyn Peryglacjalny, 24, 211–217, 1975.

Cockburn, H. A. P. and Summerfield, M. A.: Geomorphological applications of cosmogenic isotope analysis, Progr. Phys. Geogr., 28, 1–42, 2004.

Dahl, R.: Block fields, weathering pits and tor-like forms in the Narvik mountains, Nordland, Norway, Geograf. Annal., 48A, 55–85, 1966.

Dahlgren, R. A., Boettinger, J. L., Huntington, G. L., and Amundson, R. G.: Soil development along an elevational transect in the western Sierra Nevada, California, Geoderma, 78, 207–236, 1997.

Dixon, J. C. and Thorn, C. E.: Chemical weathering and landscape development in mid-latitude alpine environments, Geomorphology, 67, 127–145, 2005.

Dredge, L.: Breakup of limestone bedrock by frost shattering and chemical weathering, Eastern Canadian Arctic, Arctic Alpine Res., 24, 314–323, 1992.

Dredge, L. A.: Age and origin of upland block fields on Melville Peninsula, eastern Canadian Arctic, Geograf. Annal., 82A, 443–454, 2000.

Ericson, K.: Geomorphological surfaces of different age and origin in granite landscapes: An evaluation of the Schmidt hammer test, Earth Surf. Process. Landform., 29, 495–509, 2004.

Eriksson, B.: Data rörandeSveriges temperaturklimat (Data concerning the air temperature of Sweden). SMHI Reports, Meteorology and Climatology, RMK 39, 1982.

Fabel, D., Stroeven, A. P., Harbor, J., Kleman, J., Elmore, D., and Fink, D.: Landscape preservation under Fennoscandian ice sheets determined from in situ produced ^{10}Be and ^{26}Al, Earth Planet. Sci. Lett., 201, 397–406, 2002.

Fjeldskaar, W., Lindholm, C., Dehls, J. F., and Fjeldskaar, I.: Postglacial uplift, neotectonics and seismicity in Fennoscandia, Quaternary Sci. Rev., 19, 1413–1422, 2000.

Fjellanger, J., Sørbel, L., Linge, H., Brook, E. J., Raisbeck, G. M., and Yiou, F.: Glacial survival of blockfields on the Varanger Peninsula, northern Norway, Geomorphology, 82, 255–272, 2006.

Fredén, C. (Ed): National Atlas of Sweden: Land and soils, Sveriges Nationalatlas, Vällingby, 208 pp., 2002.

Gardner, L. R.: Long-term isovolumetric leaching of aluminum from rocks during weathering: implications for the genesis of saprolite, Catena, 19, 521–537, 1992.

Glasser, N. and Hall, A.: Calculating Quaternary glacial erosion rates in northeast Scotland, Geomorphology, 20, 29–48, 1997.

Goldstein, J., Newbury, D. E., Joy, D. C., Lyman, C. E., Echlin, P., Lifshin, E., Sawyer, L. C., and Michael, J. R.: Scanning Electron Microscopy and X-ray Microanalysis, 3rd Edn., Kluwer Academic/Plenum Publishers, New York, 689 pp., 2003.

Goodfellow, B. W.: Relict non-glacial surfaces in formerly glaciated landscapes, Earth-Sci. Rev., 80, 47–73, 2007.

Goodfellow, B. W.: A granulometry and secondary mineral fingerprint of chemical weathering in periglacial landscapes and its application to blockfield origins, Quaternary Sci. Rev., 57, 121–135, 2012.

Goodfellow, B. W., Stroeven, A. P., Hättestrand, C., Kleman, J., and Jansson, K. N.: Deciphering a non-glacial/glacial landscape mosaic in the northern Swedish mountains, Geomorphology, 93, 213–232, 2008.

Goodfellow, B. W., Fredin, O., Derron, M.-H., and Stroeven, A. P.: Weathering processes and Quaternary origin of an alpine blockfield in Arctic Sweden, Boreas, 38, 379–398, 2009.

Granger, D. E., Riebe, C. S., Kirchner, J. W., and Finkel, R. C.: Modulation of erosion on steep granitic slopes by boulder armoring, as revealed by cosmogenic ^{26}Al and ^{10}Be, Earth Planet. Sci. Lett., 86, 269–281, 2001.

Green, C. P. and Eden, M. J.: Gibbsite in the weathered Dartmoor granite, Geoderma, 6, 315–317, 1971.

Grudd, H. and Schneider, T.: Air temperature at Tarfala Research Station 1946–1995, Geograf. Annal., 78A, 115–119, 1996.

Hales, T. C. and Roering, J. J.: Climatic controls on frost cracking and implications for the evolution of bedrock landscapes, J. Geophys. Res., 112, F02033, doi:10.1029/2006JF000616, 2007.

Hall, A. M. and Phillips, W. M.: Weathering pits as indicators of the relative age of granite surfaces in the Cairngorm Mountains, Scotland, Geograf. Annal., 88A, 135–150, 2006.

Hättestrand, C. and Stroeven, A. P.: A relict landscape in the centre of Fennoscandian glaciation; geomorphological evidence of minimal Quaternary glacial erosion, Geomorphology, 44, 127–143, 2002.

Hopkinson, C. and Ballantyne, C. K.: Age and Origin of Blockfields on Scottish Mountains, Scottish Geogr. J., 130, 116–141, 2014.

Isaksen, K., Holmlund, P., Sollid, J. L., and Harris, C.: Three deep alpine-permafrost boreholes in Svalbard and Scandinavia, Permafrost Perigl. Process., 12, 13–25, 2001.

Isaksen, K., Sollid, J. L., Holmlund, P., and Harris, C.: Recent warming of mountain permafrost in Svalbard and Scandinavia, J. Geophys. Res., 112, F02S04, doi:10.1029/2006JF000522, 2007.

Ives, J. D.: Block fields, associated weathering forms on mountain tops and the Nunatak hypothesis, Geograf. Annal., 4, 220–223, 1966.

Ives, J. D.: Biological refugia and the nunatak hypothesis, in: Arctic and Alpine Environments, edited by: Ives, J. D. and Barry, R. G., Methuen, London, 605–636, 1974.

Jansson, K. N., Stroeven, A. P., Alm, G., Dahlgren, K. I. T., Glasser, N. F., and Goodfellow, B. W.: Using a GIS filtering approach to replicate patterns of glacial erosion, Earth Surf. Process Landf., 36, 408–418, 2011.

Kauffman, G., Wu, P., and Li, G.: Glacial isostatic adjustment in Fennoscandia for a laterally heterogenous earth, Geophys. J. Int., 143, 262–273, 2000.

Kleman, J. and Stroeven, A. P.: Preglacial surface remnants and Quaternary glacial regimes in northwestern Sweden, Geomorphology, 19, 35–54, 1997.

Kleman, J., Stroeven, A. P., and Lundqvist, J.: Patterns of Quaternary ice sheet erosion and deposition in Fennoscandia and a theoretical framework for explanation, Geomorphology, 97, 73–90, 2008.

Kohl, C. P. and Nishiizumi, K.: Chemical isolation of quartz for measurement of in situ-produced cosmogenic nuclides, Geochim. Cosmochim. Acta, 56, 3586–3587, 1992.

Lal, D.: Cosmic ray labeling of erosion surfaces: in situ nuclide production rates and erosion models, Earth Planet. Sci. Lett., 104, 424–439, 1991.

Lambeck, K., Purcell, A., Funder, S., Kjær, K. H., Larsen, E., and Möller, P.: Constraints on the Late Saalian to early Middle Weichselian ice sheet of Eurasia from field data and rebound modeling, Boreas, 35, 539–575, 2006.

Le Meur, E. and Huybrechts, P.: A comparison of different ways of dealing with isostasy: examples from modelling the Antarctic ice sheet during the last glacial cycle, Ann. Glaciol., 23, 309–317, 1996.

Li, Y., Fabel, D., Stroeven, A. P., and Harbor, J.: Unraveling complex exposure-burial histories of bedrock surfaces under ice sheets by integrating cosmogenic nuclide concentrations with climate proxy records, Geomorphology, 99, 139–149, 2008.

Lidmar-Bergström, K.: A long-term perspective on glacial erosion, Earth Surf. Process. Landf., 22, 297–306, 1997.

Lisiecki, L. E. and Raymo, M. E.: A Pliocene-Pleistocene stack of 57 globally distributed benthic δ^{18}O records, Paleooceanography, 20, PA1003, doi:10.1029/2004PA001071, 2005.

Marquette, G. C., Gray, J. T., Gosse, J. C., Courchesne, F., Stockli, L., MacPherson, G., and Finkel, R.: Felsenmeer persistence under non-erosive ice in the Torngat and Kaumajet mountains, Quebec and Labrador, as determined by soil weathering and cosmogenic nuclide exposure dating, Can. J. Earth Sci., 41, 19–38, 2004.

May, H. M., Helmke, P. A., and Jackson, M. L.: Gibbsite solubility and thermodynamic properties of hydroxy-aluminum ions in aqueous solution at 25 °C, Geochim. Cosmochim. Acta, 43, 861–868, 1979.

McKeague, J. A., Grant, D. R., Kodama, H., Beke, G. J., and Wang, C.: Properties and genesis of a soil and the underlying gibbsite-bearing saprolite, Cape Breton Island, Canada, Can. J. Earth Sci., 20, 37–48, 1983.

Meunier, A., Sardini, P., Robinet, J. C., and Prêt, D.: The petrography of weathering processes: facts and outlooks, Clay Min., 42, 415–435, 2007.

Milne, G. A., Mitrovica, J. X., Scherneck, H.-G., Davis, J. L., Johansson, J. M., Koivula, H., and Vermeer, M.:. Continuous GPS measurements of postglacial adjustment in Fennoscandia: 2. Modelling results, J. Geophys. Res., 109, 1–18, 2004.

Moore, D. M. and Reynolds, R. C.: X-ray Diffraction and the Identification and Analysis of Clay Minerals, 2nd Edn., University Press, Oxford, 378 pp., 1997.

Nesbitt, H. W. and Young, G. M.: Prediction of some weathering trends of plutonic and volcanic rocks based on thermodynamic and kinetic considerations, Geochimi. Cosmochim. Acta, 48, 1523–1534, 1984.

Nesje, A. and Whillans, I. M.: Erosion of Sognefjord, Norway, Geomorphology, 9, 33–45, 1994.

Nesje, A., Dahl, S. O., Anda, E., and Rye, N.: Block fields in southern Norway: Significance for the Late Weichselian ice sheet, Norsk Geologisk Tidsskrift, 68, 149–169, 1988.

Nielsen, S. B., Gallagher, K., Leighton, C., Balling, N., Svenningsen, L., Jacobsen, B. H., Thomsen, E., Nielsen, O. B., Heilmann-Clausen, C., Egholm, D. L., Summerfield, M. A., Clausen, O. R., Piotrowski, J. A., Thorsen, M. R., Huuse, M., Abrahamsen, N., King, C., and Holger Lykke-Andersen, H.: The evolution of western Scandinavian topography: a review of Neogene uplift versus the ICE (isostasy-climate-erosion) hypothesis, J. Geodynam., 47, 72–95, 2009.

Nishiizumi, K.: Preparation of ^{26}Al AMS standards, Nuclear Instrume. Methods Phys. Res. B, 223–224, 388–392, 2004.

Nishiizumi, K., Imamura, M., Caffee, M. W., Southern, J. R., Finkel, R. C., and McAninch, J.: Absolute calibration of ^{10}Be AMS standards, Nuclear Instrum. Methods Phys. Res. B, 258, 403–413, 2007.

Paasche, Ø., Strømsøe, J. R., Dahl, S. O., and Linge, H.: Weathering characteristics of arctic islands in northern Norway, Geomorphology, 82, 430–452, 2006.

Pedersen, V. K. and Egholm, D. L.: Glaciations in response to climate variations preconditioned by evolving topography, Nature, 493, 206–2010, 2013.

Peltier, W. R.: Ice age paleotopography, Science, 265, 195–201, 1994.

Peltier, W. R.: Global glacial isostasy and the surface of the ice-age Earth: the ICE-5G (VM2) Model and GRACE, Ann. Rev. Earth Planet. Sci., 32, 111–149, 2004.

Phillips, W. M., Hall, A. M., Mottram, R., Fifield, L. K., and Sugden, D.: Cosmogenic ^{10}Be and ^{26}Al exposure ages of tors and erratics, Cairngorm Mountains, Scotland: Timescales for the development of a classic landscape of selective linear glacial erosion, Geomorphology, 73, 224–245, 2006.

Potter, N. and Moss, J. H.: Origin of the Blue Rocks block field and adjacent deposits, Berks County, Pennsylvania, Geol. Soc. Am. Bull., 79, 255–262, 1968.

Rea, B. R.: Blockfields (Felsenmeer), in: The Encyclopedia of Quaternary Science, edited by: Elias, S. A., Vol. 3, Elsevier, Amsterdam, 523–534, 2013.

Rea, B. R., Whalley, B., Rainey, M. M., and Gordon, J. E.: Blockfields, old or new? Evidence and implications from some plateaus in northern Norway, Geomorphology, 15, 109–121, 1996.

Refsnider, K. A. and Miller, G. H.: Ice-sheet erosion and the stripping of Tertiary regolith from Baffin Island, eastern Canadian Arctic, Quaternary Sci. Rev., 67, 176–189, 2013.

Reynolds, R. C.: Clay mineral formation in an alpine environment, Clays Clay Mineral., 19, 361–374, 1971.

Small, E. E., Anderson, R. S., Repka, J. L., and Finkel, R.: Erosion rates of alpine bedrock summit surfaces deduced from in situ ^{10}Be and ^{26}Al, Earth Planet. Sci. Lett., 150, 413–425, 1997.

Small, E. E., Anderson, R. S., and Hancock, G. S.: Estimates of the rate of regolith production using ^{10}Be and ^{26}Al from an alpine hillslope, Geomorphology, 27, 131–150, 1999.

Staiger, J. K. W., Gosse, J. C., Johnson, J. V., Fastook, J., Gray, J. T., Stockli, D. F., Stockli, L., and Finkel, R.: Quaternary relief generation by polythermal glacier ice, Earth Surf. Process. Landform., 30, 1145–1159, 2005.

Steer, P., Huismans, R. S., Valla, P. G., Gac, S., and Herman, F.: Bimodal Plio–Quaternary glacial erosion of fjords and low-relief surfaces in Scandinavia, Nat. Geosci., 5, 635–639, 2012.

Steffen, H. and Kauffman, G.: Glacial isostatic adjustment of Scandinavia and northwestern Europe and the radial viscosity structure of the Earth's mantle, Geophys. J. In., 163, 801–812, 2005.

Steffen, H., Kauffman, G., and Wu, P.: Three-dimensional finite-element modeling of the glacial isostatic adjustment in Fennoscandia, Earth Planet. Sci. Lett., 250, 358–375, 2006.

Stone, J. O.: Air pressure and cosmogenic isotope production, J. Geophys. Res., 105, 23753–23759, 2000.

Stroeven, A. P., Fabel, D., Hattestrand, C., and Harbor, J.: A relict landscape in the centre of Fennoscandian glaciation; cosmogenic radionuclide evidence of tors preserved through multiple glacial cycles, Geomorphology, 44, 145–154, 2002.

Stroeven, A. P., Harbor, J., Fabel, D., Kleman, J., Hättestrand, C. Elmore, D., Fink, D., and Fredin, O.: Slow, patchy landscape evolution in northern Sweden despite repeated ice-sheet glaciation, Geol. Soc. Am. Special Paper, 398, 387–396, 2006.

Strømsøe, J. R. and Paasche, Ø.: Weathering patterns in high-latitude regolith, J. Geophys. Res., 116, F03021, doi:10.1029/2010JF001954, 2011.

Stumm, W. and Morgan, J. J.: Aquatic Chemistry, 2nd Edn., John Wiley and Sons, New York, 1981.

Sugden, D. E.: The selectivity of glacial erosion in the Cairngorm Mountains, Scotland, Trans. Institute of British Geographers, 45, 79–92, 1968.

Sugden, D. E.: Landscapes of glacial erosion in Greenland and their relationship to ice, topographic and bedrock conditions, in: Progress in Geomorphology: Papers in honour of D.L. Linton, edited by: Brown, E. H. and Waters, R. S., Institute of British Geographers Special Publication, Vol. 7, 177–195, 1974.

Sugden, D. E. and Watts, S. H.: Tors, felsenmeer, and glaciation in northern Cumberland Peninsula, Baffin Island, Can. J. Earth Sci., 14, 2817–2823, 1977.

Sumner, P. D. and Meiklejohn, K. I.: On the development of autochthonous blockfields in the grey basalts of sub-Antarctic Marion Island, Polar Geogr., 28, 120–132, 2004.

US Department of Agriculture: Soil Survey Manual, Agricultural Handbook No. 18. Government Printing Office, Washington D.C., 532 pp., 1993.

Walder, J. S. and Hallet, B.: A theoretical model of the fracture of rock during freezing, Geol. Soc. Am. Bull., 96, 336–346, 1985.

Watanabe, T., Funakawa, S., and Kosaki, T.: Distribution and formation conditions of gibbsite in the upland soils of humid Asia: Japan, Thailand and Indonesia, 19th World Congress of Soil Science, Soil Solutions for a Changing World, 1–6 August 2010, Brisbane, Australia, 17–20, 2010.

Wesolowski, D. J. and Palmer, D. A.: Aluminum speciation and equilibria in aqueous solution: V. Gibbsite solubility at 50 °C and pH 3–9 in 0.1 molal NaCl solutions (a general model for aluminum speciation; analytical methods), Geochim. Cosmochim. Acta, 58, 2947–2969, 1994.

Whalley, W. B., Rea, B. R., and Rainey, M.: Weathering, blockfields, and fracture systems and the implications for long-term landscape formation: some evidence from Lyngen and Øksfordjøkelen areas in north Norway, Polar Geogr., 28, 93–119, 2004.

White, A. F., Blum, A. E., Schulz, M. S., Vivit, D. V., Stonestrom, D. A., Larsen, M., Murphy, S. F., and Eberl, D.: Chemical weathering in a tropical watershed, Luquillo Mountains, Puerto Rico: I. Long-term versus short-term weathering fluxes, Geochim. Cosmochim. Acta, 62, 209–226, 1998.